REPORT DOCUMENTATION PAGE

Form Approved OMB No. 0704-0188

1. REPORT DATE *(DD-MM-YYYY)*	2. REPORT TYPE	3. DATES COVERED *(From – To)*
05-03-2007	Final Report	1 March 2006 - 01-Mar-07

4. TITLE AND SUBTITLE

TECHNICAL TESTING OF DEEP-UV SOLID-STATE SOURCES FOR FLUORESCENCE LIFETIME MEASUREMENTS IN THE FREQUENCY DOMAIN

5a. CONTRACT NUMBER
FA8655-06-1-3011

5b. GRANT NUMBER

5c. PROGRAM ELEMENT NUMBER

6. AUTHOR(S)

Professor Arturas Zukauskas

5d. PROJECT NUMBER

5d. TASK NUMBER

5e. WORK UNIT NUMBER

7. PERFORMING ORGANIZATION NAME(S) AND ADDRESS(ES)

Vilnius University
Sauletekio Ave. 9
2040 Vilnius 10222
Lithuania

8. PERFORMING ORGANIZATION REPORT NUMBER

N/A

9. SPONSORING/MONITORING AGENCY NAME(S) AND ADDRESS(ES)

EOARD
PSC 821 BOX 14
FPO AE 09421-0014

10. SPONSOR/MONITOR'S ACRONYM(S)

11. SPONSOR/MONITOR'S REPORT NUMBER(S)
Grant 06-3011

12. DISTRIBUTION/AVAILABILITY STATEMENT

Approved for public release; distribution is unlimited.

13. SUPPLEMENTARY NOTES

14. ABSTRACT

Recently, deep-ultraviolet light emitting diodes were developed basing on AlGaN materials system. These LEDs emit milliwatt fluxes at wavelengths short enough for excitation of fluorescence in basic biological fluorophores and bacterial agents. In particular, deep-UV LEDs can be used for excitation of aromatic amino acids, whereas near-UV LEDs are suitable for excitation of autofluorescent coenzymes. The SUVOS AlGaN LEDs as well as commercial InGaN near-UV LEDs were tested for spectral purity and the possibility of high-frequency modulation up to 200 MHz and applied in frequency-domain measurements of fluorescence lifetime on the nanosecond scale. Applicability of such measurements for real-time characterization of fluorescence was evaluated using an optimized automated laboratory facility for frequency-domain measurements of fluorescence lifetime. The output of the LEDs was harmonically modulated at frequencies up to 200 MHz and the phase difference between the waveforms of the excitation emission and fluorescence was measured as a function of frequency.

15. SUBJECT TERMS

EOARD, Semiconductor diodes, optical materials, Optical Sensors

16. SECURITY CLASSIFICATION OF:			17. LIMITATION OF ABSTRACT	18, NUMBER OF PAGES	19a. NAME OF RESPONSIBLE PERSON
a. REPORT	b. ABSTRACT	c. THIS PAGE			DONALD J SMITH
UNCLAS	UNCLAS	UNCLAS	UL	27	19b. TELEPHONE NUMBER *(Include area code)* +44 (0)20 7514 4953

FINAL REPORT ON PROJECT

TECHNICAL TESTING OF DEEP-UV SOLID-STATE SOURCES FOR FLUORESCENCE LIFETIME MEASUREMENTS IN THE FREQUENCY DOMAIN

Grant number: **FA8655-06-1-3011**
Submitted to: **European Office of Aerospace Research and Development**
Submitted by: **Dr. A. Žukauskas, Institute of Materials Science and Applied Research, Vilnius University, Saulėtekio al. 9-III, LT-10222 Vilnius, Lithuania**

February 2007

TABLE OF CONTENTS

SUMMARY

Recently, deep-ultraviolet (UV) light emitting diodes (LEDs) were developed basing on AlGaN materials system. These LEDs emit milliwatt fluxes at wavelengths short enough for excitation of fluorescence in basic biological fluorophores and bacterial agents. In particular, deep-UV LEDs can be used for excitation of aromatic amino acids, whereas near-UV LEDs are suitable for excitation of autofluorescent coenzymes (NADH and flavines). Such LEDs are already used in prototype fluorescence "detect-to-warn" sensors of hazardous biological agents. Furthermore, simple means of high-frequency modulation of LEDs allow for devising of low-cost sensors with the discrimination ability improved through real-time measurements of fluorescence decay time, which is a unique "fingerprint" of a biological compound.

This project was aimed at the evaluation of currently most advanced deep-UV LEDs developed under SUVOS Program for measurement of fluorescence lifetime signatures in *B. globigii* spores (simulant of hazardous biological agent *B. anthracis*), natural autofluorophores, and typical airborne interferants.

The SUVOS AlGaN LEDs as well as commercial InGaN near-UV LEDs were tested for spectral purity and the possibility of high-frequency modulation up to 200 MHz and applied in frequency-domain measurements of fluorescence lifetime on the nanosecond scale. Applicability of such measurements for real-time characterization of fluorescence was evaluated using an optimized automated laboratory facility for frequency-domain measurements of fluorescence lifetime. Fluorescence lifetime was shown to be resolved for fluorophore concentrations as low as ~10^{-8} mol/l what might be sufficient to distinguish between different chemical and biological compounds in accumulated extended samples of airborne particles.

A matrix of fluorescence spectral and phase signatures of dry *B. globigii* spores and common interferants (albuminous, epithelium, and cellulosous materials as well as aromatic hydrocarbons and mineral building materials) was obtained for the UV LEDs with eight different emission wavelengths (255–375 nm). The output of the LEDs was harmonically modulated at frequencies up to 200 MHz and the phase difference between the waveforms of the excitation emission and fluorescence was measured as a function of frequency. Basing on the analysis of the data matrix, a new concept of a "detect-to-warn" biofluorescence sensor with a high ability of discrimination of bioparticles against most common interferants was proposed.

1. INTRODUCTION

Recently, sensing of chemical and biological agents received a considerable interest because of increasing threats of attacks using biological warfare agents from uncontrolled terrorist nets and military units sponsored by rogue political regimes. Continuous monitoring of large areas for protection of both military and civilian populations requires a compact, low-maintenance and inexpensive "detect-to-warn" sensors of aerosol bioparticles operating in real time and featuring early warning capability, high probability of detection of hazardous agents, and low false alarm rate.

To that end, optical methods of bioparticle sensing are addressed with increasing interest.[1] These methods offer fast and *in situ* detection and identification of numerous compounds employing a variety of techniques, such as elastic and inelastic scattering of light, absorbance, fluorescence, Raman, and breakdown emission spectroscopy.[2] In particular, measurements of spectral and excitation characteristics of fluorescence excited by UV radiation is already a well established analytical technique for detect-to-warn sensors of airborne bioparticles with a fast response and high discrimination ability.[3,4] Several directions in the development of fluorescence sensors evolved. One of the directions is based on a single particle interrogation, which requires highly collimated excitation beams provided exclusively by lasers. However despite the crucial role of gas-discharge and solid-state lasers in analytical spectroscopy, these devices still remain quite expensive, heavy, and bulky sources of light with high power consumption and high maintenance.

Another direction in detect-to-warn fluorescence sensors is based on accumulation of extended samples which allows for use of sources of incoherent light. The latter approach offers considerably lower price and size of a sensor at some expense in discrimination ability. Insufficient discrimination ability is the main drawback of both approaches resulting in an inadmissibly high false alarm rate. In both cases, this drawback is somewhat mitigated in matured systems that contain means of preselection of particles within a particular range of sizes using elastic scattering of light. Nevertheless, for the development of highly reliable bioparticle sensor networks for detect-to-warn purposes, further improvement in discrimination ability of the fluorescence measurements is required.

Inexpensive, compact, lightweight, and low-maintenance emitters of incoherent UV radiation are light-emitting diodes (LEDs). LEDs differ from lasers, including semiconductor laser diodes, in that the emission has a short coherence length and cannot be completely collimated and focused to a small area what is preferable for individual analysis of micrometer-size particles. However in comparison with lasers, LEDs are available in a wider wavelength range, feature longer lifetimes and no abrupt failure, have stable output and low noise, produce little heat, can be flexibly assembled in arrays, and are much cheaper. Recently, semiconductor-based UV sources of light became available owing to a tremendous progress in nitride semiconductor technology.[5] In particular, UV LEDs are being developed based on $Al_xGa_{1-x}N$ alloy, which can be tailored for wavelengths ranging from 360 to 200 nm depending on Al molar fraction x.[6] This wavelength range exactly matches the excitation spectra of most important natural autofluorophores contained in biological agents, such as bacteria, spores, and viruses. Although suffering from low coherence length that is insufficient for obtaining high density of optical power for single-particle interrogation and remote sensing, LEDs are already used in numerous prototype sensor systems.[7–9] Moreover, UV LEDs can not only match the excitation spectra of important biofluorophores but offer inexpensive solutions for measurement of fluorescence decay time, which is an informative characteristics of a biological object. Fluorescence decay time provide with information on structure and environment of molecular compounds and can serve as additional component of the fluorescence identification vector for improving of the sensor performance in terms of probability of correct detection.

Advanced UV LEDs operating in the spectral range relevant to biofluorescence excitation were developed under SUVOS program. One of the most successful developments was a set of AlGaN UV LEDs commercialized by Sensor Electronic Technology, Inc. (Columbia, SC). These UV LEDs are widely used in prototype detect-to warn sensors, operating on the regime of analysis of fluorescence intensity and spectral properties. However, less attention is paid to measurements of fluorescence lifetime.

This project was aimed at the evaluation of currently most advanced deep-UV LEDs developed under SUVOS Program for measurement of fluorescence lifetime in natural autofluorophores and biological compounds as well as in typical interferants, such as cellulose-containing materials, diesel fuel, mineral materials, etc. The LEDs were tested for the possibility of high-frequency modulation up to 200 MHz and applied in frequency-domain measurements of fluorescence lifetime on the nanosecond scale. Applicability of such measurements for real-time characterization of fluorescence in multi-mode-operation sensors with improved probability of correct detection was evaluated.

The report is organized as follows. Section 2 contains some background information on theoretical and instrumental issues of fluorescence lifetime measurements. Section 3 deals with the spectral and high-frequency characterization of the LEDs under testing. In Section 4, a detailed description of the experimental setup used in this work is presented. Section 5 is devoted to the main results of the project, investigation of spectral and decay-time characteristics of fluorescence in a stimulant *B. globigii* and numerous possible interferants. In Section 6, the main conclusions of the work are drawn.

2. BACKGROUND INFORMATION

In this section, a brief introduction to time-domain and frequency-domain measurements of fluorescence lifetime is presented. Section 2.1 deals with theoretical background of fluorescence lifetime measurements, whereas some important instrumental issues for both measurement modes are discussed in Section 2.2.

2.1. Theoretical background

Fluorescence can be characterized by an intensity response function, $I(t)$, which relates to the structure and environment of molecular compounds. The response function can have various forms depending on the nature and complexity of electronic excitation, relaxation and recombination. In the simplest case of a single fluorophore with one type of radiative residue, the response function under moderate excitation is single-exponential,

$$I(t) = \alpha \exp(-t/\tau) \ , \tag{1}$$

where α is the preexponential factor (zero-time intensity) and τ is the decay time. For a mixture of fluorophores and/or a fluorophore containing several types of radiative residues, the response function is multi-exponential,

$$I(t) = \sum_i \alpha_i \exp(-t/\tau_i) \ . \tag{2}$$

where α_i are the corresponding fractional contributions of each fluorophore/residue to the total emission. In a disordered system where the excitation experiences random walk before reaching a radiative site, the response function is stretched-exponential,

$$I(t) = \alpha \exp(-t/\tau)^{\beta} \ , \tag{3}$$

where β is the fractal dimension of the random walk. Under high excitation conditions typical of a pulsed-laser application, bimolecular annihilation of excitations may take place. This results in a complex response function,

$$I(t) = \frac{\alpha \exp(-t/\tau)}{1+\alpha\gamma\tau\left[1-\exp(-t/\tau)\right]}, \tag{4}$$

where γ is the bimolecular annihilation constant. At short delays ($t \ll \tau$), Eq. (4) yields a hyperbolic response.

The form of the fluorescence intensity response function is unique for a fluorophore in a particular environment. Fluorescence due to biofluorophores usually is well described by single-exponent or multi-exponent intensity response functions, which can be characterized by a single or multiple fluorescence lifetimes, respectively.

Basically, fluorescence lifetime measurements can be carried out in two ways.[10] The first one, which is widely used in spectroscopy and practical applications, is based on short-pulse excitation with subsequent tracing of temporal distribution of fluorescence (time-domain measurement). The second, alternative, approach is based on using of harmonically modulated quasi-continuous excitation and measuring of the phase shift and/or decrease in the modulation depth of the fluorescence signal (frequency-domain measurement).

Figure 1 displays principles of the two fluorescence lifetime measurement modes.[10] In the time-domain mode (Fig. 1a), the excitation pulse is followed by an asymmetric fluorescence pulse. The decay of the fluorescence intensity, which mimics the intensity response function, can be traced and directly monitored. For a particular decay pattern, the response function is commonly parameterized using an appropriate plot. For instance for a single-exponent response function, the fluorescence lifetime can be extracted from a semilogarithmic plot by measuring the angle of the decay slope,

$$\tau = -\left[\frac{\partial \ln I(t)}{\partial t}\right]^{-1} . \tag{5}$$

Note that the time where Eq. (5) is applicable must be much larger than the duration of the excitation pulse and the fluorescence rise time. In most practical applications, the latter is much shorter than the decay time. However, the duration of the excitation pulse can be comparable or even longer than the fluorescence lifetime. In this case the measured temporal profile of fluorescence, $I_k(t)$, is a convolution of the fluorescence intensity response function and the temporal profile of the excitation pulse measured with the same instrument, $L(t)$,

$$I_k(t) \propto \int_{-\infty}^{t} I(t-t')\, L(t')\, dt' . \tag{6}$$

To extract the fluorescence lifetime from a convoluted experimental data, a complex deconvolution procedure is to be performed.

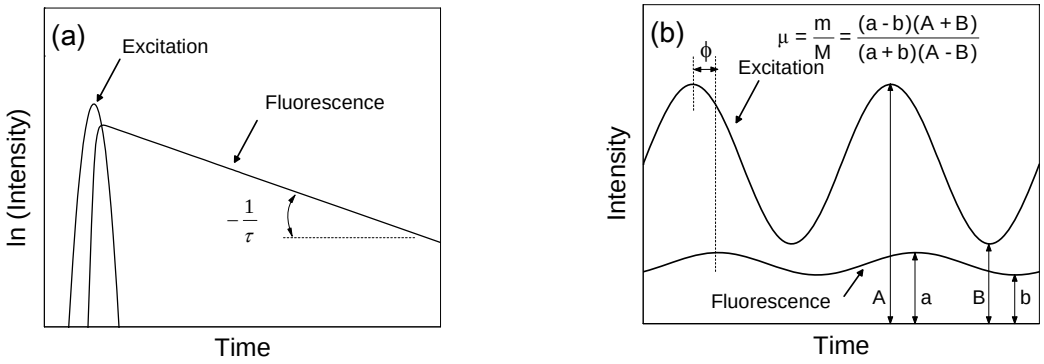

Fig. 1. Time-domain (a) and frequency-domain (b) fluorescence lifetime measurements. (After Ref. 10).

Excitation of fluorescence by harmonically modulated sources enables one to extract fluorescence lifetime through measurement of the difference in phase and modulation of the excitation and fluorescence signals. The principle of the frequency-domain measurement is illustrated in Fig. 1b. The excitation source is modulated by a harmonic (sinusoidal) waveform at an angular frequency ω and modulation depth *M*. The resulting fluorescence signal is modulated at the same frequency and modulation depth *m*. However, because of the fluorescence delay in respect of the excitation, the fluorescence signal is phase-shifted by a phase angle ϕ and the modulation depth is decreased by a demodulation factor μ. For an arbitrary fluorescence intensity response function, the phase shift is

$$\phi(\omega) = \arctan(N_\omega / D_\omega) \tag{7}$$

and the demodulation factor is

$$\mu(\omega) = \sqrt{N_\omega^2 + D_\omega^2} , \tag{8}$$

where the sine and cosine transformations of the response function are

$$N_\omega = \int_0^\infty I(t) \sin \omega t \; dt \Big/ \int_0^\infty I(t)\, dt \tag{9}$$

and

$$D_\omega = \int_0^\infty I(t) \cos \omega t \; dt \Big/ \int_0^\infty I(t)\, dt , \tag{10}$$

respectively. The phase shift and demodulation factor can be defined for a variety of response functions, although analytical expressions are available only for some cases. Generally, experimental data on the phase shift and modulation factor is to be acquired in a wide range of frequencies and the parameters of the response function are to be extracted by a fitting procedure using the method of nonlinear least squares. In particular, for a multi-exponent decay,

$$N_\omega = \frac{\sum_i \frac{a_i \omega \tau_i^2}{1+\omega^2 \tau_i^2}}{\sum_i a_i \tau_i} \tag{11}$$

and

$$D_\omega = \frac{\sum_i \frac{a_i \tau_i}{1+\omega^2 \tau_i^2}}{\sum_i a_i \tau_i} \ . \tag{12}$$

For instance for a two-exponent decay, the fitting procedure involves three independent parameters, namely, τ_1, τ_2, and α_1 (the second contribution is considered to be dependent, since $\alpha_2 = 1 - \alpha_1$).

In the case of a single-exponent response function, the phase shift and demodulation factor are coupled to the fluorescence lifetime by simple functional relations

$$\phi(\omega) = \arctan(\omega\tau) \tag{13}$$

and

$$\mu(\omega) = \left(1+\omega^2\tau^2\right)^{-1/2} \ , \tag{14}$$

respectively. In the latter case, fluorescence lifetime can be determined form a single measurement of the phase shift or modulation factor at an appropriate frequency, i.e., there is no need to perform measurements in a wide frequency range. This allows one to measure fluorescence lifetime in real time. If the form of the response function is *a priori* unknown, the phase shift at a single frequency can still serve as a fingerprint of the fluorophore under investigation, however.

2.2. Instrumental issues

Actually, the two fluorescence lifetime measurement modes are mutually related to each other trough Fourier transform and the data obtained contains the same information on the fluorescence response function. However, from the point of view of designing of the excitation and detection systems, data processing, compactness, and cost-efficiency these two modes have both advantages and disadvantages in respect of each other. Below, some considerations on these issues are presented.

An inexpensive source for time-domain fluorescence lifetime measurements is flashlamp, which can generate light pulses as short as 1 ns. Flashlamps emit in a wide spectral range, which depends on the gas used. The main drawbacks of flashlamps in fluorescence lifetime measurements are low spectral density of the emission, low repetition rate, high voltage used, unstable output power and time profile, and pulsed electrical interference.

Historically, laser induced fluorescence (LIF) usually based on ion, excimer, and solid-state lasers is the most developed analytical technique with a fast response, high temporal and spatial resolution, and ability of remote sensing.[3,4] Pulsed gas-discharge and solid-state lasers are stable, can operate at high repetition rates, and offer high flexibility in tailoring of the excitation wavelength with the absorption spectrum of fluorophores. The latter advantage is due to the availability of nonlinear-crystal and dye converters of wavelength, which operate in the high-power regime. For instance, the third (λ = 354 nm) and the fourth (λ = 466 nm) harmonics of a widespread yttrium-aluminum garnet laser can be used for excitation of common coenzymes and protein amino acids, respectively. Advanced systems employing solid-state lasers with parametric converters and equipped with multichannel spectral analyzers can provide with extended spectroscopic data on fluorescence of various biological agents and interferents.[11] However, pulsed ion, excimer, and solid-state lasers still remain quite expensive, heavy, and bulky sources of light with high power consumption and high maintenance. Some types of solid-state and gas discharge lasers can operate in the cw regime. For a frequency-domain measurement, a cw laser equipped with an electro-optic or acousto-optic modulator is required.[10] The capital and operating price of such a system usually is of the same order as that of the pulsed one.

Considering LEDs and LDs, which usually can be operated in both pulsed and high-frequency harmonical modes by simple modulation of the driving current, the quasi-continuous regime might be preferable, since at a comparable average output power the pulsed device experiences a higher peak electrical and optical stress that facilitates its aging. Note that LEDs differ from lasers in that the emission has a short coherence length and cannot be completely collimated and focused to a small area what is preferable for individual analysis of micrometer-size particles. However in comparison with LDs, LEDs are available in a wider wavelength range, feature longer lifetimes and no abrupt failure, have stable output and low noise, produce little heat, can be

flexibly assembled in arrays, and are cheaper. These advantages of LEDs are already utilized in numerous applications of optical measurement technology.[2,10,12]

The price of the detection system in pulsed measurements increases especially in the subnanosecond region, where either optical shutters, up- and down-converters of wavelength, streak cameras or high-speed photodetectors combined with wide-band electronics are required.[10] Besides, pulsed sources usually produce electrical interference due to abrupt breakdown in the gas, voltage and current switching, etc. Meanwhile in the frequency domain regime, the detector can operate at frequencies even above the cut-off frequency provided that the signal is still detectable. Also, phase shifts that are shorter than the rise time of the detection system can be resolved and measurements can be cheapened using relatively simple and conventional electronic means of frequency downconversion.

Finally, in time-domain measurements, fluorescence lifetime is typically extracted by accumulation and processing of numerous data points. For fluorescence lifetimes comparable with the duration of the excitation pulse and the detector response time, the processing is complicated by the deconvolution procedure, which also requires measurement of the excitation pulse waveform with a high precision. Contrarily, measurement of phase, which is utilized in the frequency-domain technique, is a well established technique that enables one to acquire the decay-time signature from a single data point. Instead of the deconvolution procedure, the instrumental response function can be taken into account by a simple subtraction of the overall phase shift introduced by the elements of the measurement system. This is preferable in cost-efficient detectors operating in real-time regime. However in the frequency-domain mode, elimination of the harmonic interference from the source driving circuit and of the background fluorescence due to light scattered in to the detector directly from the excitation source is a more complex procedure in comparison with a simple subtraction of the interference and background used in the time-domain mode. Therefore a deeper electrical and optical isolation of the detector from the source is required to prevent the cross-talk.

Both time-domain and frequency-domain measurements can be conducted for levels of fluorescence as low as discontinuous single-photon fluxes (e.g., using time-correlated photon counting technique).[10,13] In this case, the time of appearance of each single photon after the zero-time or zero-phase moment, respectively, is to be recorded and numerous data are to be accumulated. The accumulated data can be sorted as a function of either time or phase and the lifetime can be extracted using numerical processing. Actually, in the single-photon counting regime the two measurement techniques instrumentally coalesce and the difference is only in the algorithm of data processing. Again, in the frequency-domain regime, taking in to account of the instrumental distortion can be simpler since one needs only subtraction of the phase bias rather than deconvolution of the fluorescence response function against the excitation pulse as in the time-domain regime. Meanwhile, elimination of the fluorescence background and electrical interference is simpler in the time-domain mode. For a particular LED or LD, which can be used in either mode, the sensitivity of the measurement in the two regimes might be different depending on the difference of the average power delivered in either pulsed of quasi-continuous mode. (Typically, boosting of the pulsed current over the steady-state value results in an unpredictable competition between an increased carrier leakage over quantum wells and suppression of nonradiative recombination due to enhanced bimolecular recombination.)

The considerations presented above imply that the frequency-domain mode of fluorescence lifetime measurements might have some important advantages in respect to the time-domain mode when an LD or LED is used for excitation. In particular, provided that no high spatial resolution and remote sensing is required, UV LEDs, which are cheaper and available within a wider range of wavelengths than LDs, are perfect candidates for real-time frequency-domain fluorescence lifetime measurements in compact and inexpensive biofluorescence sensors with improved discrimination ability.

Time-domain fluorescence lifetime measurements in biological compounds and agents using 340-nm and deep-UV 280-nm UV LEDs have been already demonstrated.[14–16] Recently, deep-UV LEDs were applied for biofluorescence lifetime measurements in the frequency-domain mode.[17–19]

3. CHARACTERIZATION OF UV LEDs

Deep UV LEDs used in this study have been developed at Sensor Electronic Technology, Inc. (SETI) under support from Defense Advanced Research Project Agency (Program Manager Dr. J. Carrano). Detailed information on the LEDs design and growth procedures is presented in Refs. 20–23.The UV LED structures were grown in a custom-designed vertical metalorganic chemical vapor deposition (MOCVD) system, with trimethyl aluminum (TMA), trimethyl gallium (TMG), silane, Cp2-Mg, and NH_3 as precursors and basal plane

sapphire as substrates. The high quality AlN buffer and AlGaN-based superlattices for strain management were grown using our novel Migration Enhanced MOCVD (MEMOCVD™) technique. Optimization of MEMOCVD™ growth yielded high-quality AlN buffers and AlN/AlGaN superlattices with the full width at half maximum ≤ 9 arcsec for AlN x-ray diffraction (0002) ω-scan. LED patterns with various area/perimeter ratios were designed and mesa type devices were fabricated. Flip-chip packaging with massive contact bumps facilitated light extraction through a UV-transparent sapphire substrate and efficient heat removal.

The UV LEDs obtained from SETI (UVTOP® brand) were specified for the emission peaks important for the excitation of biofluorescence (255 nm, 270 nm, 280 nm, 300 nm, 320 nm, and 340 nm; ±5 nm) and 0.4 to 2.5 mW output power at 20 mA driving current. For comparison, mass-production InGaN-based UV LEDs (Nichia Europe BV, Amsterdam, the Netherlands) specified for 365 nm (NSHU590B) and 375 nm (NSHU590A) peak wavelengths were investigated.

3.1. Spectral properties of UV LEDs

Spectral characteristics of LEDs used for fluorescence excitation are important in terms of the possibility to spectrally isolate fluorescence from excitation. For frequency-domain measurement such a separation is especially important, since a parasitic cross-talk between the excitation and fluorescence circuits results in a phase shift error that cannot be eliminated by simple subtraction. To estimate the level of the LED emission in the spectral range relevant to biofluorescence, the electroluminescence spectra were measured within a wide dynamic range of intensities.

High-intensity-contrast emission spectra of the LEDs were measured by using a calibrated double monochromator with a low level of stray light (JY HRD1) and a UV-enhanced photomultiplier (Hamamatsu R1463P) operating in the photon-counting mode. The calibration of the spectral response of the measurement system was performed using standardized tungsten and deuterium lamps (Bentham CL2 and CL3, respectively).

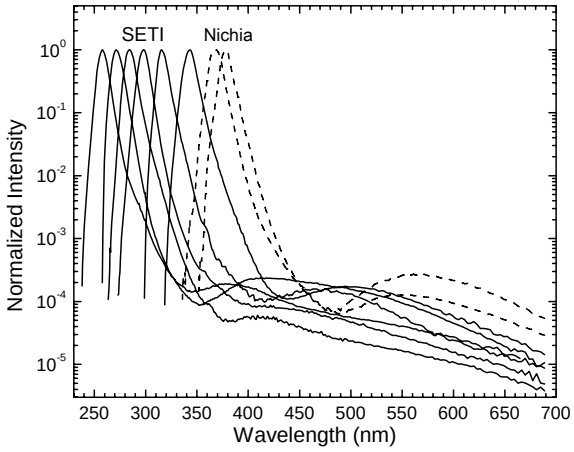

Fig. 2. Normalized spectral power distribution of UVTOP® series deep-UV AlGaN LEDs (solid lines) and near-UV Nichia InGaN LEDs (dashed lines).

Figure 2 shows the emission spectra within a dynamic range of over 5 orders of magnitude for the LEDs driven at 20 mA. The spectra peak at 258 nm, 271 nm, 282 nm, 298 nm, 315 nm, and 343 nm for the SETI LEDs and at 368 nm and 378 nm for the Nichia LEDs, respectively. The full width at half magnitude of the line is about in the range of 10 to 12 nm for the SETI LEDs and about 11 to 13 nm for the Nichia LEDs, respectively. The emission line is asymmetric and a long-wavelength wing ranging throughout the entire visible spectrum is observed. Such wings are typical of nitride-based LEDs and originate from the exponential band tail of localized states due to band potential fluctuations in the AlGaN and InGaN alloys as well as from impurity-mediated optical transitions within the semiconductor band gap. The intensity of the far long-wavelength background is seen to constitute about 10^{-4} of that at the peak and about 10^{-3} of the spectrally integrated intensity. To our estimate, such a high spectral purity can be employed in fluorescence measurements using a pair of mutually extinguishing optical filters to optically isolate fluorescence from the excitation emission and to ensure a low cross-talk between the excitation and detection electronic circuits. Depending on the level of fluorescence signal, either standard color-glass optical filters or more expensive custom-designed interference filters can be used.

3.2. Modulation properties of UV LEDs

To evaluate the applicability of the LEDs for fluorescence lifetime measurements in the frequency domain, modulation characteristics were measured. Modulation of the device at higher frequencies enables one to measure shorter fluorescence lifetimes with higher sensitivity and accuracy.

Modulation characteristics of the LEDs were measured at a bias of 20-mA dc current and an rf power of +5 dbm applied from a high-power signal generator (Aeroflex IFR 2023A). The optical signal was detected by a Hamamatsu H6780-01 photomultiplier with a risetime of 0.78 ns and the ac component of the response was digitized by a radio-frequency lock-in amplifier (Stanford Research Systems SR844).

Figure 3 shows the modulation characteristics of the SETI and Nichia LEDs in the frequency range of 25 kHz–200 MHz. (The swings of about 5% are due to the measurement set-up.) The SETI LEDs exhibit a pronounced modulated emission up to the frequency of 200 MHz. The cut-off frequencies are from 110 to 170 MHz for the SETI LEDs and about 20 MHz for the Nichia LEDs. The modulation ability for the SETI AlGaN LEDs is somewhat wider than those of Nichia InGaN LEDs. The AlGaN and InGaN LEDs have similar noise characteristics[24] and can be used for measurement of phase shifts between the excitation and fluorescence waveforms in the frequency range up to ~100 MHz that is sufficient for extraction of fluorescence decay time in the subnanosecond range relevant to biofluorophore identification.

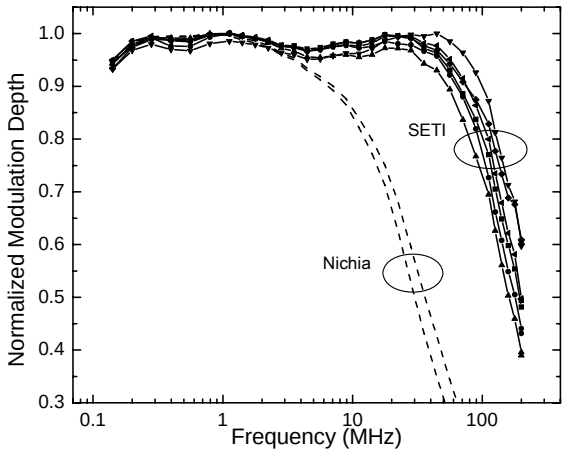

Fig. 3. Modulation characteristics of of UVTOP® series deep-UV AlGaN LEDs (solid lines) and near-UV Nichia InGaN LEDs (dashed lines).

4. EXPERIMENTAL SETUP

In this section, the experimental setup for measurement of fluorescence decay time in the frequency domain using UV LEDs is described. In Section 4.1, the design of the setup is described. In Section 4.2, verification of the setup by measurements of fluorescence lifetime in standard fluorophores (organic dyes and their mixtures) is presented.

4.1 Setup design

Figure 4 shows the block diagram of the optimized laboratory facility employed in our work. The design of the facility is based on the fluorescence phase-shift measurements using a radio-frequency lock-in amplifier.[25]

The LEDs were driven using a bias tee (Picosecond 5547) at a dc current of 20 to 30 mA provided by a regulated current source (homemade, based on LM317 voltage regulator). For the modulation of the LED current (from +5 to +15 dbm; 0.1 to 200 MHz), a high-power digital signal generator with a low phase jitter (Aeroflex IFR 2023A) was used. The long-wavelength background of the LED emission was filtered out using a short-pass filter (SPF). The UV emission of the LED was focused using a fused-silica lens and guided to a sample using a custom-made dichroic mirror (DM). Dichroic mirrors with the transition wavelength of 295 nm and 395 nm were used for the detection of fluorescence in the near-UV and blue-green regions, respectively. Fluorescence from the sample was passed through the dichroic mirror, filtered by a long-pass filter (LPF) and focused on the cathode of a photomultiplier (PMT). The optically filtered fluorescence signal was detected by a PMT with a risetime of 0.78 ns (Hamamtsu H6780-01). A wide-band preamplifier (Hamamatsu C5594; 36 dB) was used for

increasing of the sensitivity of the detection arm. The amplified electrical signal was branched into ac and dc components using a second bias tee (Picosecond 5547). These components were fed into a radio-frequency lock-in amplifier (Stanford Research Systems SR844) and used for measurement of the phase and modulation depth of the fluorescence.

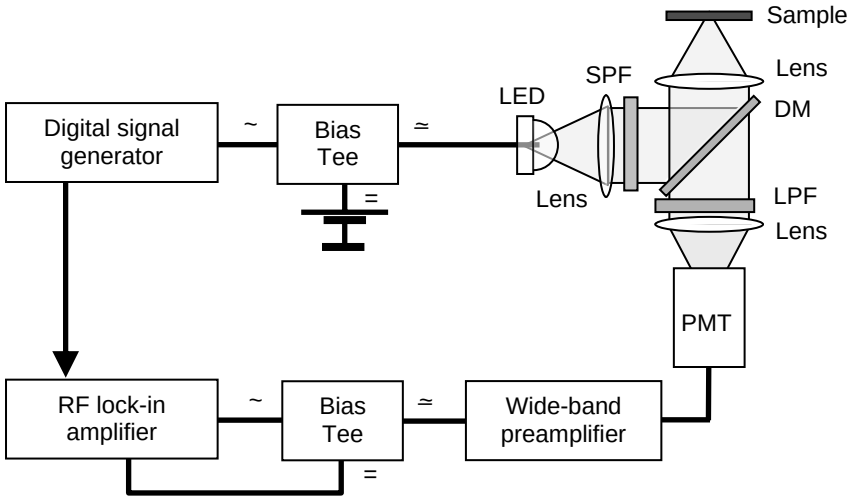

Fig. 4. Block-diagram of the laboratory facility for fluorescence lifetime measurements using UV LEDs.

The sets of the LPF and SPF filters were carefully designed for each type of LEDs used. A Schott UG11 glass or a custom made interference filter with a cut-off wavelength of 285 nm stood for LPFs for LEDs emitting at 300 nm, 320 nm, and 340 nm and at 255 nm, 270 nm, and 280 nm, respectively. For measurements in the blue-green region, a stack of Schott BG25 and GG420 glass filters was used as an LPF, whereas for measurements in the near-UV region, the stack contained a custom made interference filter with a cut-off wavelength of 310 nm and a Schott UG1 glass filter. All custom-made dichroic mirrors and interference filters were manufactured by Optida Ltd., Vilnius. Figures 5a and b depict the normalized spectral power distribution of the LEDs' emission incident on sample (solid lines) and the transmittance of the detection arm for measurements using 340-nm and 280-nm LEDs, respectively. One can see that in both cases, optical isolation between the excitation and detection arms of at least of four orders of magnitude was achieved for the SPF/DM/LPF filter sets used. Such optical isolation is important for frequency-domain fluorescence lifetime measurements to prevent the undesired cross-talk between the modulated source and detector as discussed in Section 2.2.

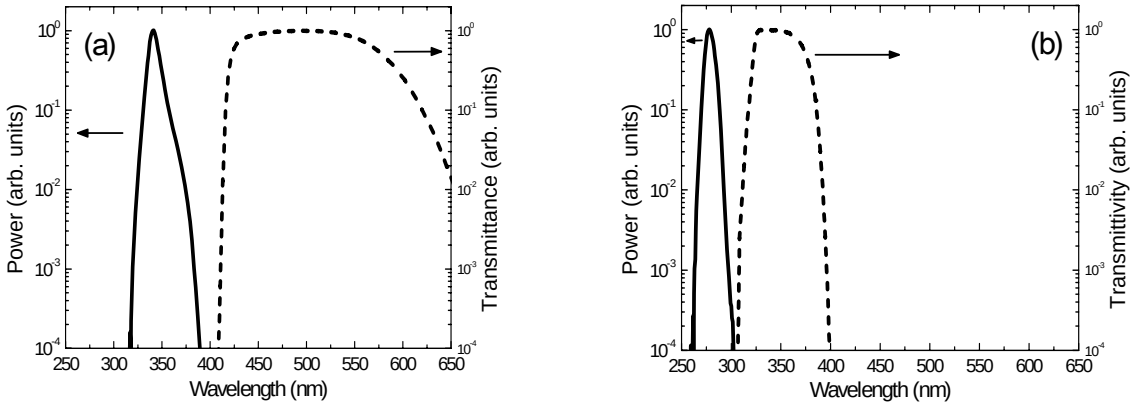

Fig. 5. Spectral power distribution of UV radiation incident on sample (solid lines) and transmittance of the detection arm (dashed lines) for the measurement setup using 340-nm (a) and 280-nm (b) LEDs.

The system was also verified for the negligibility of electrical cross-talk between the excitation and detection branches by obscuring the LED and measuring the magnitude of the residual signal in the entire frequency range. In all subsequent measurements of fluorescence lifetime, the harmonic interference from both the optical and electrical cross-talk was preserved well below 1%. A typical relative systematic error in fluorescence lifetime due to such a crosstalk is approximately equal to the percentage of the parasitic rf signal in the detected one.[26]

The lock-in amplifier and the digital signal generator were linked to personal computer using a GPIB interface. A LabVIEW tool (Fig. 6) was created to automate the measurement procedure and to process the data. The tool allowed for setting of the number of points and the measurement time per point, automated measurement of the fluorescence phase and modulation depth in a preset frequency range, multiple data acquisition, accumulation, averaging and visualization, and generation of a datasheet (phase and modulation depth vs. frequency) file. The datasheet is passed to an ORIGIN7.5 C-macros that allowed for the elimination of the instrumental error in phase shift due to the delays in the PMT and electronics, graphical representation of the data, and extraction of the fluorescence lifetimes and fractional intensities by the least-squares method.

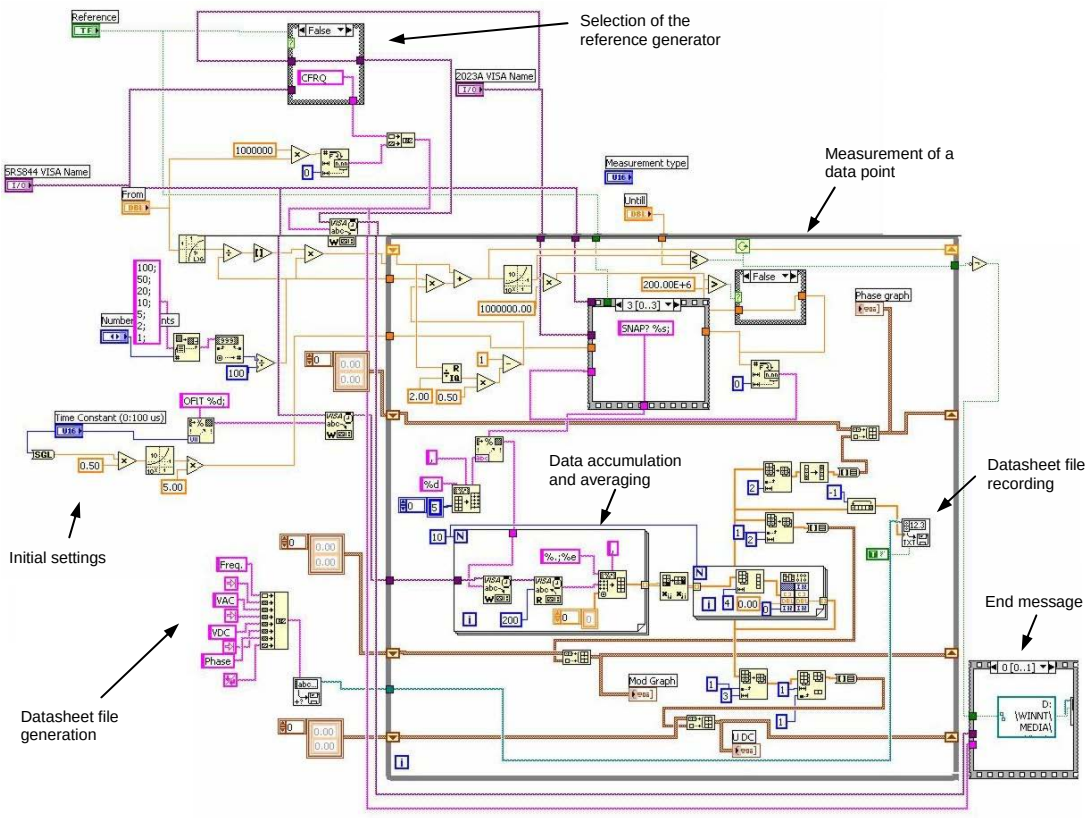

Fig. 6. Block-diagram of the LabVIEW tool for automation of the fluorescence lifetime measurements in the frequency domain.

4.2 Verification of the measurement system

The developed experimental setup vas verified by performing measurements of fluorescence lifetimes in standard fluorophores, such as organic dyes and their mixtures.

The fluorescence lifetime measurement procedure was as follows. First, a scattering metal plate was placed instead of the sample and the phase and modulation depth of excitation was measured as a function of frequency with the LPF removed (residual emission of a LED that passed the dichroic mirror was utilized for measurements). Then the LPF was returned and the phase and modulation depth of fluorescence the samples was measured as a function of frequency. Finally, the difference in phase and the ratio of modulation depth of the fluorescence in respect of the excitation was determined. Since both the excitation and fluorescence dependences were equally affected by the frequency response characteristic of the experimental setup, the obtained differential data was free of instrumental distortion. To extract the fluorescence lifetime, the measured frequency dependences of the demodulation factor and phase shift were fitted to a single-exponent or two-exponent model using the least-square method.

Figure 7 depicts typical results of the measurement of fluorescence lifetime in common ultraviolet organic dyes BMQ (a) and P-terphenyl (b). The dyes (Lambdaphysik, Goettingen, Germany) were dissolved in hexane at a concentration of 1×10^{-6} mol/l. A 280-nm LED was used for excitation and fluorescence was detected through the 320-nm LPF. The measurement time per point was 500 ms and the data was averaged over 10 scans. Filled

and open points are the experimental data on the modulation depth and phase shift of fluorescence in respect of the excitation waveform, respectively. Lines show the least-squares fits to a two-exponent decay pattern. The fit revealed single-exponent decay with the lifetimes of 0.90 ns for BMQ and 1.06 ns for P-terphenyl with the fitting accuracy of about 1.5%.

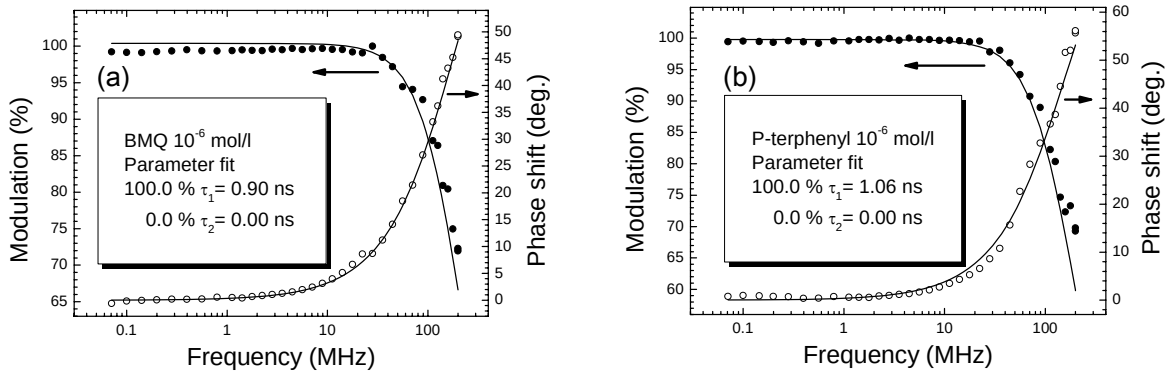

Fig. 7. Fluorescence modulation depth and phase shift vs. frequency in respect of the excitation waveform in BMQ (a) and P-terphenyl (b) in hexane under 280-nm LED excitation. Points, experiment; lines, least-squares fit with a single-exponent decay pattern.

The accuracy of the measurement was limited by a crosstalk between the excitation and detection arms of the facility as mentioned above. In the example presented, the percentage of the parasitic signal in respect of the fluorescence signal was about 0.15%. Since the systematic error in fluorescence lifetime due to a crosstalk is approximately equal to the percentage of the parasitic rf signal in the detected one, this suggests that for fluorophore concentrations as low as 5×10^{-8} mol/l, fluorescence lifetime can still be resolved with a reasonable reliability (3%) that is sufficient to distinguish between different chemical and biological compounds.

Figure 8 shows the results of the measurement in another organic dye Coumarin 440 (Exciton, Dayton, OH) dissolved in ethanol (2.5×10^{-5} mol/l). A 340-nm LED was used for excitation and fluorescence was detected through the blue-green LPF. The measurement time per point was 500 ms and the data was averaged over 10 scans. Filled and open points are the experimental data on the modulation depth and phase shift of fluorescence in respect of the excitation waveform. Lines show the least-squares fits that reveal single-exponent decay with a lifetime of 3.84 ns with the fitting accuracy of 0.7%.

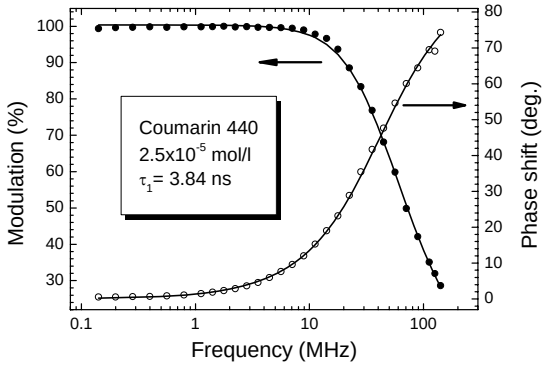

Fig. 8. Fluorescence modulation depth and phase shift vs. frequency in respect of the excitation waveform in Coumarin 440 excited by a 340-nm LED. Points, experiment; lines, least-square fit with a single-exponent decay pattern.

Figure 9 shows the results of the measurements in aqueous solutions of two organic dyes, Rhodamine 101 (a) and Quinine sulphate (b) (Exciton, Dayton, OH) at a concentration 2.5×10^{-5} mol/l. Figure 5c shows the results for the mixture of these solutions with a ratio of 1:2. A 340-nm LED was used for excitation and fluorescence was detected through the blue-green LPF. The measurement time per point was 500 ms and the data was averaged over 10 scans. Filled and open points are the experimental data on the modulation depth and phase shift of fluorescence in respect of the excitation waveform. The frequency-domain dependences for Rhodamine 101 reveal a single-exponent decay with the lifetime of 4.12 ns. In Quinine sulphate, a two-exponent decay 20.1 ns (92.3%) and 2.99 ns (7.7%) was extracted from the measured dependences. In the mixture, the accuracy of the fit allowed to extract a two-exponent decay with the lifetimes of 4.48 (95%) and 28.2 (5%). Some discrepancy in respect of the unmixed solutions was attributed to the mutual influence of the dyes on the pH of the mixture and possible chemical interaction.

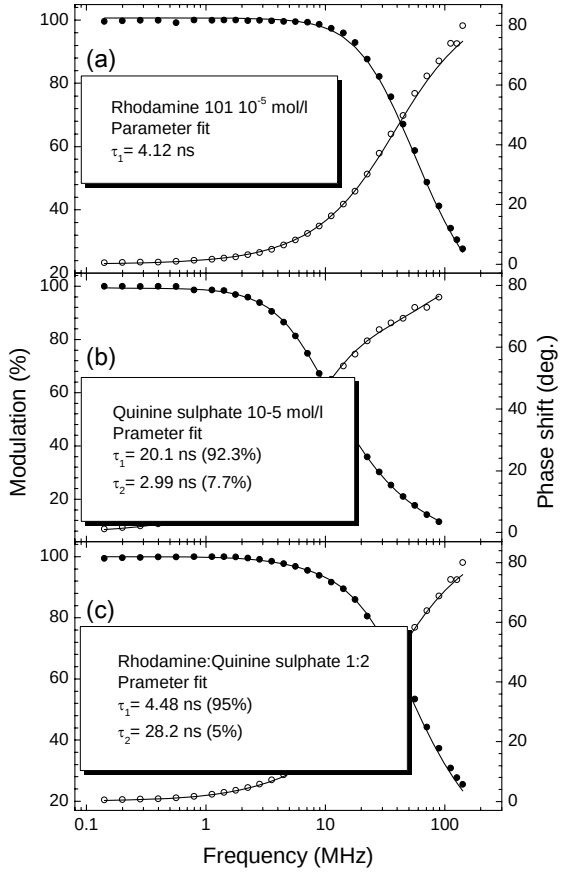

Fig. 9. Fluorescence modulation depth and phase shift vs. frequency in respect of the excitation waveform in Rhodamine 101 (a) and Quinine sulphate (b) in water excited by a 340-nm LED. (c) Same for the 1:2 mixture of the solutions. Points, experiment; lines, least-square fit.

5. IDENTIFICATION OF BIOLOGICAL AGENTS FLUORESCENCE USING UV LEDs

In this section, the results on the identification of *B. globigii* spores (an optical stimulant of dangerous biological agent *B. anthracis*) using fluorescence excited by the UV LEDs under testing are presented. Both fluorescence spectral and decay characteristics were employed for the identification and the possibility of the discrimination of the spores against common interferants that can constitute airborne particles was evaluated.

In Section 5.1, a general scheme of the acquisition of the data matrix is presented. In Section 5.2, the investigated materials are described. Section 5.3 contains data on fluorescence excitation in *B. globigii*. In Section 5.4, fluorescence spectra and phase shifts of *B. globigii* are collated with those of common interferants. In Section 5.5 discrimination charts are presented and a concept of an optimized fluorescence sensor is proposed.

5.1. Data Matrix

To evaluate the applicability of the UV LEDs for the discrimination of biofluorescence against common interferants, a matrix of fluorescence spectral and lifetime data was built. The matrix contained data on fluorescence excited in dry *B. globigii* spores and in a number of common organic and inorganic interferants (albuminous, epithelium, and cellulosous materials as well as aromatic hydrocarbons and mineral building materials) using a set of SUVOS deep-UV AlGaN LEDs and Nichia near-UV InGaN LEDs with the peak wavelengths ranging from 255 nm to 375 nm.

Hazardous biological agents, such bacteria, viruses, toxins, and fungi contain fluorescent compounds that can be identified by an optical sensor. Proteins contain three fluorescent aromatic amino acids tryptophan, tyrosine, and phenylalanine, which absorb light in the UV-C region. Tryptophan and tyrosine have the lowest absorption peaks at about 280 nm and 274 nm, respectively, whereas excitation of phenylalanine requires somewhat shorter wavelength of about 257 nm. Bacterial agents, which are either vegetative cells or spores, also contain fluorescent coenzymes (compounds involved in cell metabolic processes) such as nicotinamide adenine dinucliotide (NADH) and flavins. The lowest absorption band in NADH peaks at about 340 nm (UV-A region),

whereas flavins have absorption bands in the range of 350 to 470 nm. One more important biofluorophore, which is present only in spores rather than in vegetative cells, is dipicolinic acid (DPA) and its Ca^{2+} complex (CaDPA). DPA absorbs light around 360 nm and emits at about 440 nm.[27] These considerations imply that deep-UV (255–280-nm) LEDs enable one to photoexcite protein fluorophores, whereas near UV (300–375-nm) LEDs can be used for excitation of coenzymes and DPA.

Figure 10 shows the general diagram of the acquisition of the fluorescence data matrix. UV LEDs of eight different emission wavelengths specified above were individually applied to excite fluorescence in *B. globigii* spores and in five groups of common interferants. Eventually for each type of LED, a set of fluorescence spectra was recorded and a set of fluorescence phase shift vs. frequency dependences was obtained. For deep-UV LEDs (255–280 nm), these dependences were measured for two spectral windows (peaked at 320 nm and 450 nm), whereas for the rest LEDs (300–375 nm) only the blue window (450 nm) was employed.

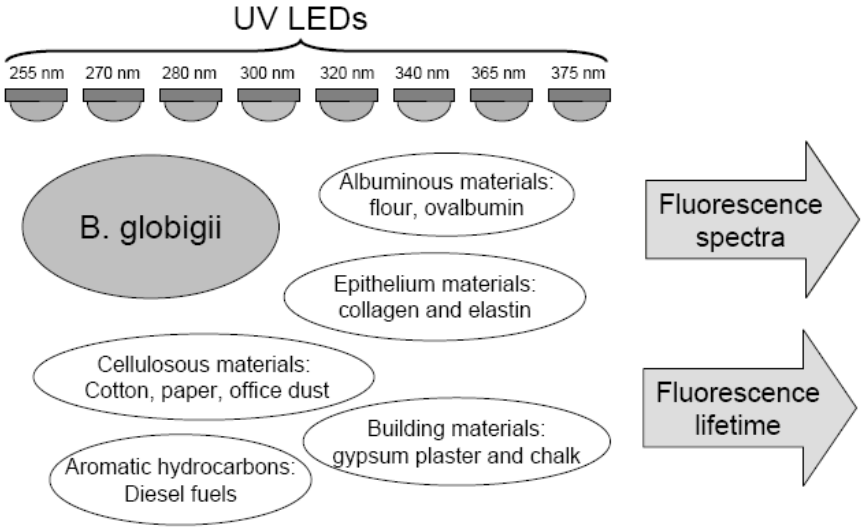

Fig. 10. General diagram of the acquisition of fluorescence data matrix. Eight types of LEDs were used for excitation of fluorescence in *B. globigii* spores and common airborne interferants. The output of the experiment is the fluorescence spectra and fluorescence lifetime (represented by fluorescence phase shift in respect of the excitation waveform).

Fluorescence spectra were resolved using a calibrated low-stray-light double monochromator (JY HRD1) and recorded using a UV-enhanced photomultiplier operating in the photon counting mode (Hamamatsu R1463P). The fluorescence spectra were fairly well resolved at about 30 to 40 nm below the peak of the LED emission spectrum. Some fluorescence spectra obtained under UV-LEDs excitation were compared with those obtained for excitation at 325 nm provided by a He–Cd laser. Despite of a lower excitation flux, the fluorescence spectra obtained by using the deep UV-LEDs exhibited reasonable intensities with a comparable or even higher signal-to-noise ratio. The latter advantage of LEDs is due to randomness of the spontaneous photon emission exclusively within intrinsic Poisson distribution what allows for achieving of the limiting value of the signal-to-noise ratio $N_s^{1/2}$ (N_s is the number of signal counts).[28,29] Note, that efficient LEDs can exhibit even lower noise due to fluctuation squeezing below Poisson distribution when driven by stable current.[30]

5.2 Materials

Spores from *B. globigii* (also, *B. antrophaeus*) ATCC 9372 (BAG-Biologische Analysen System GmbH, Germany) were produced by bacteria sporulation.[31] The bacteria were sporulated by incubation either in liquid or on solid modified Schaeffer‘s sporulation medium (2×SG)[32] at 37 °C for 3 days. Liquid cultures were incubated with vigorous aeration in a rotary shaker. Progress through sporulation was monitored microscopically by scoring for the presence of phase-bright spores and by measuring the percentage of cells in a culture that were capable of surviving a heat treatment (60°C for 30 min). The liquid cultures or the washes of the growth from the agar surfaces with sterilized deionised water were harvested by centrifugation (10,000 g, 10 min, 4 °C), stored in a cold room, and the spores were purified by repeated rounds of centrifugation and washing with cold deionised water over a period of 1–2 weeks (the duration of washing depended upon the appearance of the supernatant and

the spore pack). During the washing procedures, the spores were kept chilled. Cleaned spores were stored until use as suspensions of 10^{10} to 10^{11} CFU/ml in deionised water at 4 °C protected from light. The viable titres of spore preparations were determined by serial 10-fold dilution in 0.1 M Na phosphate buffer (pH 7.0) and plating on 2×SG solidified with 2.0% agar. For fluorescence measurements, a dense spore suspension was spotted on a quartz glass and dried out in air at a temperature of –5 °C.

Natural biofluorphores contained in bacterial spores such as aromatic amino acids (derivatives of tyrosine and tryptophan), coenzymes NADH and riboflavin as well as dipicolinic acid (DPA) were used for the analysis of the fluorescence spectral and decay-time signatures of *B. globigii*.

Several groups of typical airborne interferants such as albuminous, epithelium, and cellulosous materials as well as aromatic hydrocarbons and mineral building materials were investigated. Common albuminous interferants were represented by ovalbumin (stimulant of viral particles) and wheat flour (stimulant of high-protein-content food particles). Epithelium-originated interferants were imitated by elastin and collagen (proteins that are found in skin). Cellulosous interferants were represented by purified cotton, various kinds of paper that contain cellulose of different chemical treatment and age, and office dust extracted from the filter of an air conditioning system. Diesel fuels (both of winter and summer brands) stood for hydrocarbon interferants and chalk and gypsum plaster were used as examples of calcium carbonate based and calcium sulphate based fluorescent building materials, respectively.

Analytical-grade chemicals were used: L-tyrosine and NADH (Carl Roth GmbH, Karlsruhe, Germany), N-acetyl-L-tryptophanamide (NATA), ovalbumin, collagen and elastin (Sigma-Aldrich, St. Louis, MO), riboflavin (Reanal, Budapest, Hungary), DPA (Sigma-Aldrich, Fluka, China). L-tyrosine, NATA, NADH and riboflavin were dissolved in phosphate buffer (50 mM, pH 7.2) and the prepared solutions had the molar concentration of about 400 μM. Fluorescence measurements of ovalbumin, collagen, elastin and DPA were carried out using powdered forms.

Other interferants such as diesel fuels of several brands, wheat flour, several types of paper, cotton, office dust, and mineral building materials were obtained from utility sources and investigated in their natural form.

5.3. Fluorescence of *B. globigii*

Figure 11 shows typical fluorescence spectra of *B. globigii* (a) and natural autofluorophores contained in spores (b) under excitation using LEDs with different peak wavelengths.

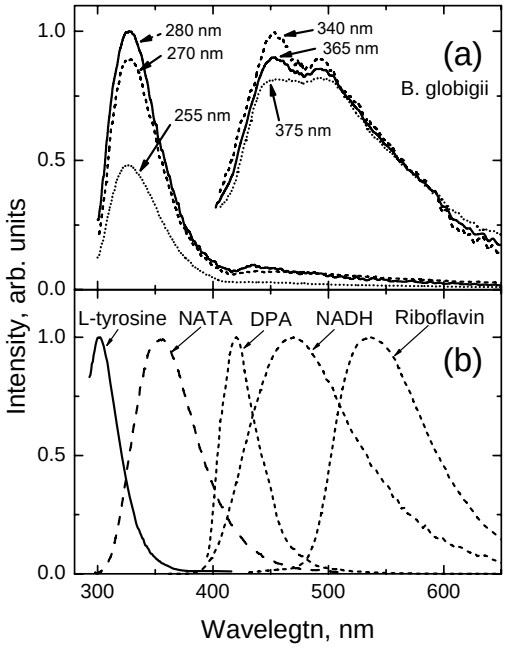

Fig. 11. (a) Fluorescence spectra of *B. globigii* spores under excitation using LEDs with different peak wavelengths (indicated). The intensities of the spectra in the two groups (255 nm/270 nm/280 nm and 340 nm/365 nm/375 nm) are normalized to the incident power. (b) Normalized fluorescence spectra of L-tyrosine and NATA (280-nm excitation) and DPA, NADH, and riboflavin (365-nm excitation).

Under 255-nm, 270-nm, and 280-nm excitation, fluorescence spectra of *B. globigii* are dominated by a band peaked at 325 nm (Fig. 11a, left). This near-UV band is due to protein amino acids, tyrosine and tryptophan. Although the peak position of the near-UV band is very close to that of unbound tyrosine in aqueous solution (Fig. 11b), the observed fluorescence is probably dominated by the tryptophan emission.[5] This is a

common situation in biological objects where the tyrosine emission is usually quenched by the energy transfer to tryptophan, whereas the tryptophan emission in nonpolar environment inside the protein globule displays a blue shift to about 316–317 nm.[33] Also under deep-UV (255–280 nm) excitation, a weak band at about 440 nm can be resolved. Under excitation using the 300-nm LED, only the long-wavelength wing of the near-UV band can be observed, whereas for the 320-nm LED, this band is completely overlapped by the excitation line (these spectra are not shown in Fig. 11a). Under 340-nm, 365-nm, and 375-nm excitation, two bands peaked at about 450 nm and 500 nm can be resolved in the fluorescence spectra of *B. globigii* spores (Fig. 11a, right). These bands in the blue-green region can be attributed to fluorescence of DPA, NADH, and flavins, and (Fig. 11b).[5,34,35] Since the peaks observed in the *B. globigii* spectra can be shifted in respect of those observed in unbound fluorophores due to an inhomogeneous environment, it is difficult to unambiguously assign the blue-green emission to particular autofluorophores. Nevertheless, the most probable assignment is that the blue band in *B. globigii* is mainly due to DPA and NADH, whereas the green band is due to flavins.

Figure 3 shows some typical results of the fluorescence phase shift under 280-nm excitation measured within the 320-nm spectral window and under 365-nm excitation measured in the 450-nm spectral window. (Under 280-nm excitation, the signal in the 450-nm spectral window for most of the materials investigated was weak and a high accuracy was difficult to attain.) Both under 280-nm and 365-nm excitation, *B. globigii* spores exhibit phase shift vs. frequency dependences that reveal two-exponent fluorescence decay with the lifetimes in the subnanosecond and nanosecond range (Fig. 3a). Bacterial autofluorophores have single-exponent decay patterns,[18] except DPA, which exhibits a two-exponent decay (Fig. 3b). Since under 280-nm excitation the dependence for *B. globigii* was obtained within the 320-nm spectral window, both the short (0.89 ns) and the long (3.6 ns) components of the fluorescence lifetime are to be attributed to tryptophan in two different environments.[10,36] Under 365-nm excitation, the shorter component of the lifetime in *B. globigii* (0.60 ns) is probably contributed by NADH or the shorter component of DPA, whereas the longer component of *B. globigii* (7.9 ns) is probably due to flavins and the longer component of DPA.[10,35,37]

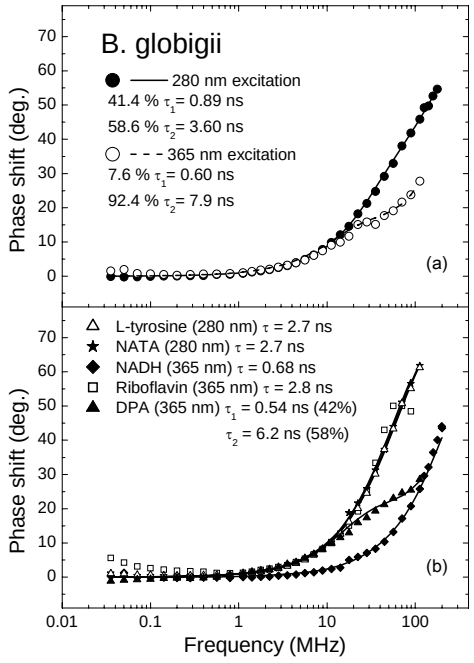

Fig. 12. Dependences of fluorescence phase vs. modulation frequency in *B. globigii* spores (a) under 280-nm (filled points) and 365-nm (open points) excitation and in bacterial autofluorphores (b) L-tyrosine (open triangles) and NATA (stars) under 280-nm excitation; NADH (diamonds), riboflavine (sqauares), and DPA (filled triangles) under 365-nm excitation. Data for 280-nm and 365-nm excitation was obtained within 320-nm and 450-nm spectral windows, respectively. Points, experiment; lines, the least-squares fit to single-exponent (L-tyrosine, NATA, NADH, and riboflavin) and two-exponent (*B. globigii* and DPA) fluorescence decay.

5.4. Discrimination of *B. globigii* against common interferants

Below we discuss a part of the obtained fluorescence data matrix for two most important excitation wavelengths, 280 nm and 365 nm. The selection of these wavelengths was based on the following considerations. Three deep-UV LEDs with the wavelengths of 255 nm, 270 nm, and 280 nm, which match the spectral region of protein absorption, yielded almost identical results both in spectral and phase-shift characterization of *B. globigii* spores and the interferants. Of those three LEDs, the 280-nm one excites near-UV fluorescence in the spores with the highest efficiency. Also under 280-nm excitation, fluorescence in the blue region has somewhat higher relative

intensity than under 255-nm and 270-nm excitation. Therefore, the 280-nm excitation wavelength was selected as the most appropriate one for further discussion in more detail.

The 300-nm and 320-nm LEDs were ruled out because of difficulties in isolation of excitation and fluorescence in the near-UV region and a low intensity of the excited fluorescence in the blue region. All three rest LEDs (340 nm, 365 nm, and 375 nm) are suitable for excitation of fluorescent coenzymes. These three excitation wavelengths resulted in almost identical fluorescence phase shifts. However, with increasing excitation wavelength in the 340-375 nm range, the peak intensity of the blue band somewhat decreases, whereas the relative contribution of the green band increases (Fig. 11a). Also it should be noted that in comparison with the 340-nm AlGaN LEDs, the 365–375-nm InGaN LEDs resulted in somewhat higher signal-to-noise ratio of fluorescence due to a higher output flux. Eventually, based on the trade-off between the overall fluorescence intensity and green to blue fluorescence intensity ratio, which is related to the informativeness of the spectra, as well on the signal-to-noise ratio, the 365-nm LED was selected for the further discussion as the most appropriate one.

Figure 13 shows fluorescence spectra (a to d) and phase dependences (e and f) of *B. globigii* spores vs. cellulosous materials (typical paper, pure cotton, and office dust) under 280-nm (solid lines) and 365-nm (dashed lines) LED excitations. As discussed above, fluorescence spectra of *B. globigii* (Fig. 13a, which contain same data as Fig. 11a) reveal that under 280-nm excitation *B. globigii* spores exhibit an intense peak in the near-UV region (around 325 nm) due to tryptophan and a rather weak emission in the blue-green region. It is to be noted that a high ratio of near-UV to blue-green emission is typical of highly washed spores and can be much smaller in spores that are less refined. A typical characteristic of fluorescence spectra of the cellulosous materials (Figs. 13b to d) is a broad band peaked in the blue region (around 440 nm) with extended wings in both UV and green regions.[38] Although different cellulosous materials exhibit different ratios of the blue to near-UV and blue to green intensities, basically the near-UV and green wings are always weaker in intensity than the blue peak. For 365-nm LED excitation, two peaks in the fluorescence spectra of *B. globigii* spores can be clearly resolved (at about 450 nm and 500 nm), whereas the cellulosous materials show broad bands in the same blue-green region. Obviously, the blue-green emission of the spores is difficult to distinguish from that of the cellulosous materials, especially by low spectral resolution detectors used in inexpensive fluorescence sensors.

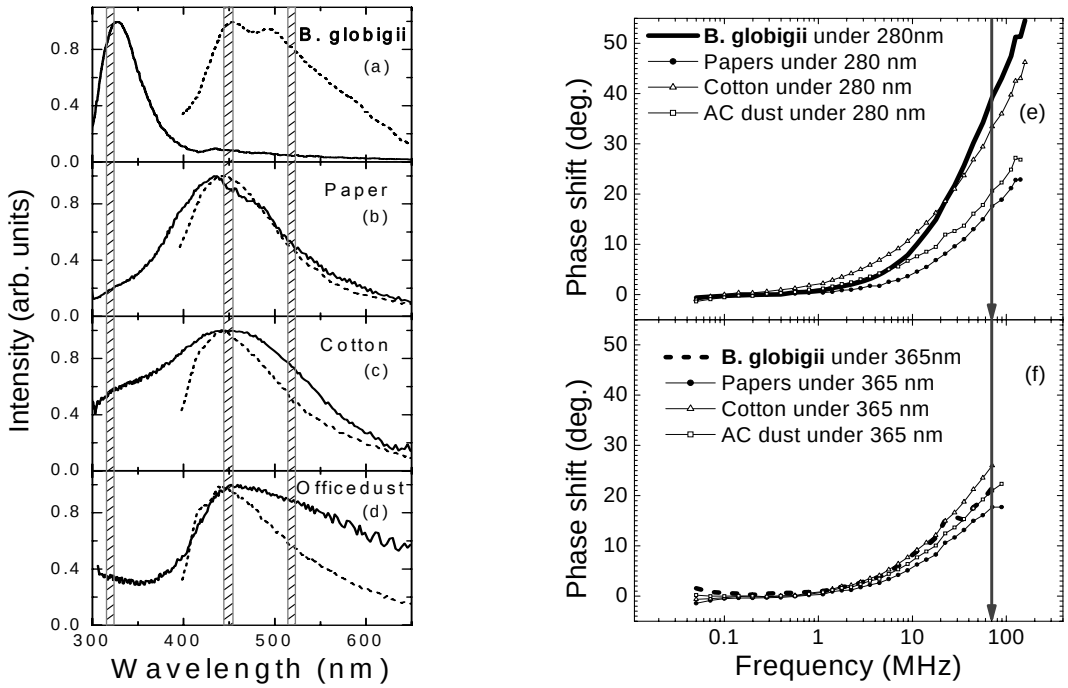

Fig. 13. Fluorescence spectra of *B. globigii* spores (a) vs. cellulosous materials paper (b), cotton (c) and AC dust (d) under 280-nm (solid line) and 365-nm (dashed line) excitation. Phase shift under 280-nm (e) and 365-nm (f) excitation as a function of frequency for *B globigii* spores (solid line for 280-nm excitation, dashed line for 365-nm excitation), paper (filled circles), cotton (open triangles) and AC dust (open squares).

Figures 13e and f show the results of the measurement of the fluorescence phase in *B. globigii* spores vs. the cellulosous materials. For 280-nm excitation (Fig. 13e), such substances as paper and office dust exhibit

much smaller phase shifts, i.e. smaller fluorescence decay times, than the spores. Pure cotton has higher values of the phase shift, but still below that of the spores. For 365-nm excitation (Fig. 13d), the phase vs. frequency dependence of *B. globigii* spores overlaps with those of the cellulosous materials and no discrimination can be performed.

Fluorescence spectra of *B. globigii* spores are compared with those of the epithelium materials in Fig. 14a to c. Under 280-nm excitation (solid lines), both elastin (Fig. 14b) and collagen (Fig. 14c) have intense features in the near-UV region (around 310 nm), probably due to tryptophan in the environment somewhat different from that in the spores.[10,36] In the blue region, these compounds exhibit a broad band that is much more intense than the blue one in the washed spores. Under 365-nm excitation (dashed lines), the epithelium materials show an intense band in the blue region (around 440 nm) with a broad wing extending in to the green region.[35] Although the blue-to-green fluorescence intensity ratio is somewhat higher in the epithelium materials that in the washed spores, this ratio is difficult to exploit as a reliable discrimination parameter taking into account the sensitivity of the fluorescence spectra of the spores to the preparation conditions.

Comparison of the fluorescence phase in the spores with that in the epithelium materials reveals a strong overlap under 280-nm excitation (Fig. 14d) despite different environments of tryptophan. Our data matrix shows that this overlap can be partially mitigated with shifting of the excitation to shorter wavelengths (e.g., 255 nm), however no high discrimination can still be achieved. Contrarily, under 365-nm excitation, the epithelium materials show much larger phase shifts in comparison with those in the spores. We attribute such a difference to a completely different origin of the blue emission in collagen and elastin, which is due to pyridinoline groups.[39]

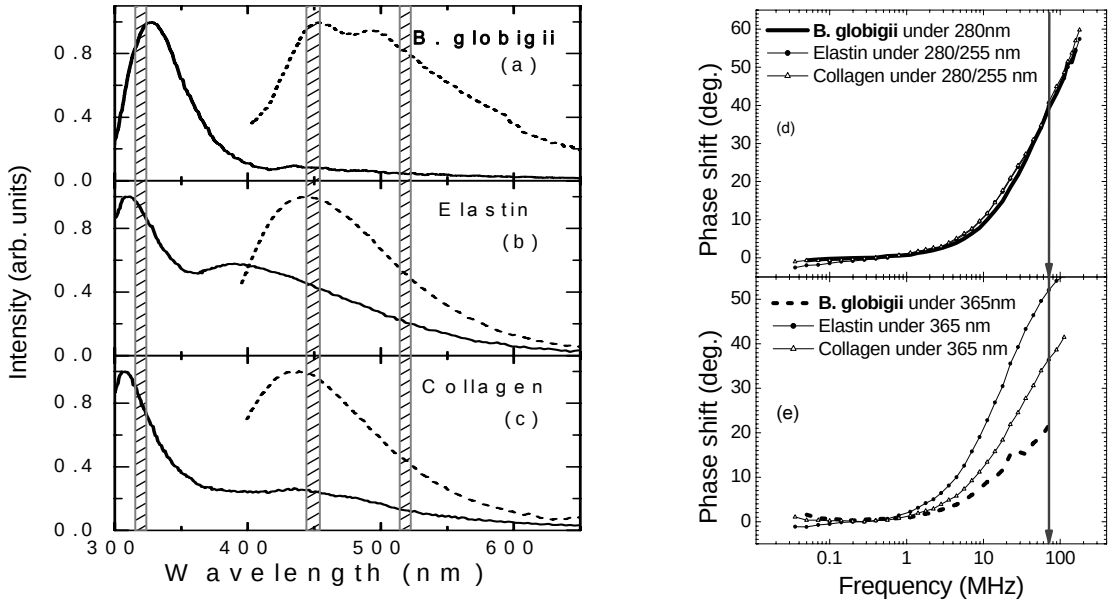

Fig. 14. Fluorescence spectra of *B. globigii* spores (a) vs. epithelium materials elastin (b) and collagen(c) under 280-nm (solid line) and 365-nm (dashed line) excitation. Phase shift under 280-nm (d) and 365-nm excitation as a function of frequency for *B. globigii* spores (solid line for 280-nm excitation, dashed line for 365-nm excitation), elastin (filled circles) and collagen (open triangles).

Figures 15a to c show fluorescence spectra of *B. globigii* vs. albuminous materials. Under 280-nm excitation (solid lines), both ovalbumin (Fig. 15b) and flour (Fig. 15c) exhibit fluorescence spectra with an intense peak at about 330 nm. These spectra are dominated by emission of protein[10,36] and are very similar to that of the spores (Fig. 15a). Under 365-nm excitation (dashed lines), the albuminous materials feature a single blue band peaked at about 440 nm. Due to the absence of a green band, the blue-to-green intensity ratio is somewhat higher than in the spores, however we suggest that these differences are too small to provide with reliable discrimination in low spectral resolution sensors.

Figure 15d and e show the results on the fluorescence phase shift measurements for the two excitation wavelengths. Under 280-nm excitation (Fig. 15d), lower phase shifts for *B. globigii* spores can be clearly resolved in comparison with ovalalbumin and flour. Under 365-nm excitation, such a difference in phase shifts can be even higher.

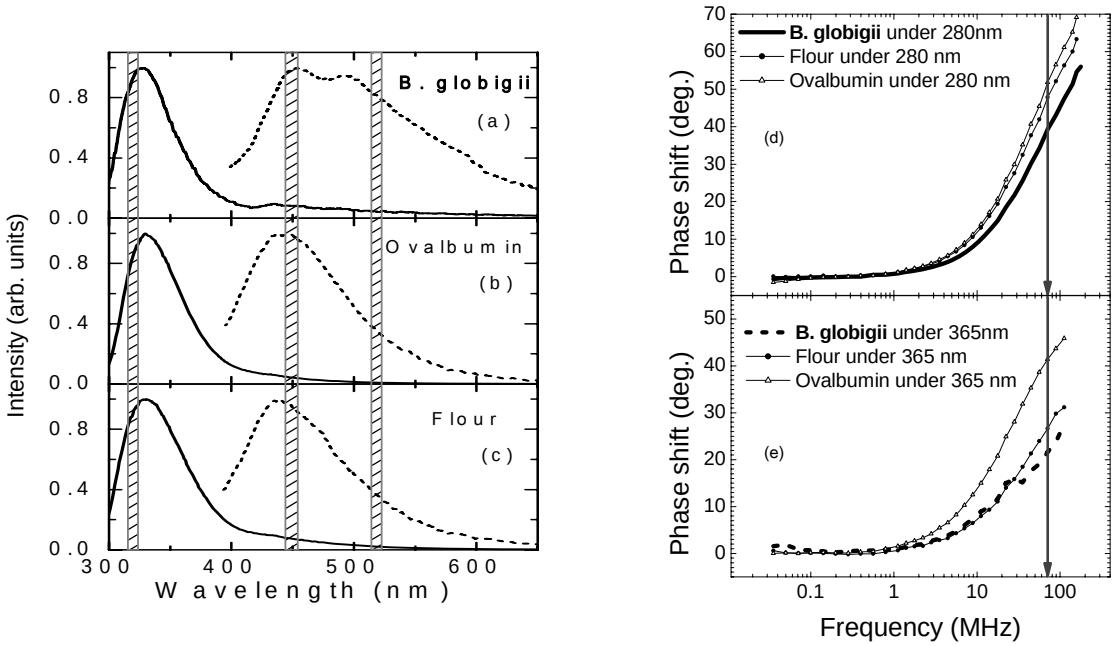

Fig. 15. Fluorescence spectra of *B. globigii* (a) vs. albuminous materials ovalbumin (b) and flour (c) under 280-nm (solid line) and 365-nm (dashed line) excitation. Phase shift under 280-nm (d) and under 365-nm (e) excitation as a function of frequency for *B. globigii* (solid line for 280-nm excitation, dashed line for 365-nm excitation), ovalbumin (open triangles) and flour (filled circles).

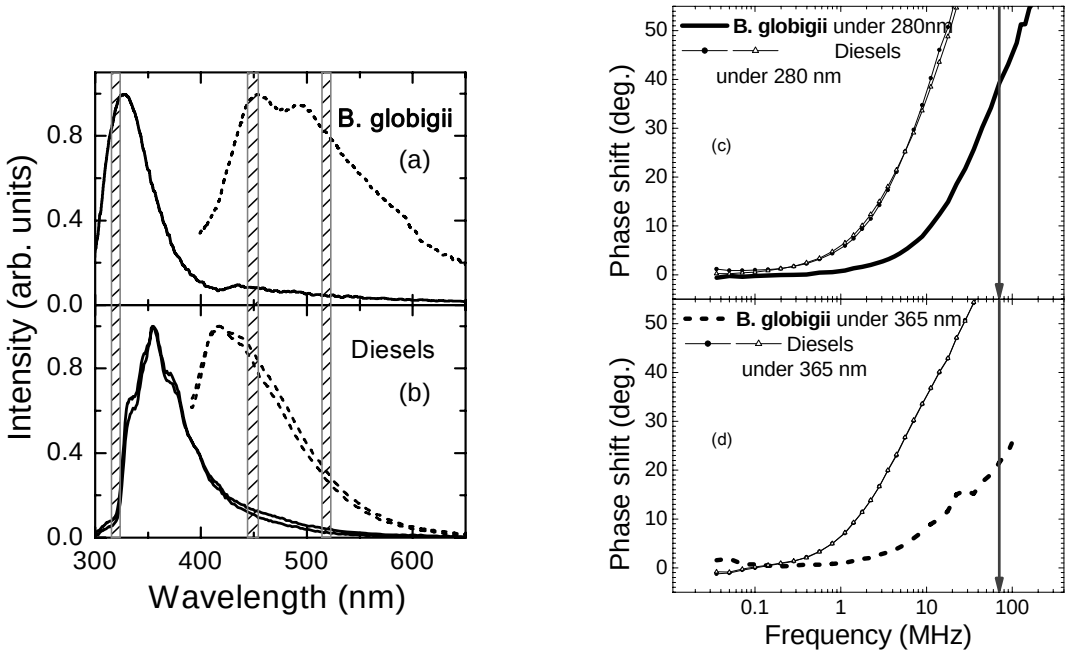

Fig. 16. Fluorescence spectra of *B. globigii* (a) vs. two kinds of diesel fuel materials (b) under 280-nm (solid line) and 365-nm (dashed line) excitations. Phase shift under 280-nm (c) and 365-nm (d) excitation as a function of frequency for *B. globigii* (solid line for 280-nm excitation, dashed line for 365-nm excitation) and two kinds of diesels (filled circles and open triangles).

Figures 16a and b show fluorescence spectra of *B. globigii* spores vs. diesel fuels under 280-nm (solid lines) and 365-nm (dashed lines) excitation. For 280-nm excitation, the fluorescence spectra of diesel fuels (Fig. 16b) have a well-resolved band peaked at about 355 nm with an extended long-wavelength wing. Since this band, which is due to aromatic rings of hydrocarbons,[40] is shifted to longer wavelengths in comparison to the tryptophan band (Fig. 16a), the near-UV to blue intensity ratio is much lower than that for the spores. This difference in the near-UV to blue intensity ratio can be somewhat smaller in sensors with a low spectral resolution because of the proximity of the 355-nm band to the center of the 320-nm window, however.

Fluorescence spectra of diesels under 365-nm LED excitation feature a band at about 420 nm. Again, the blue-to green intensity ratio is quite different from that of *B. globigii* spores and can be used for discrimination.

Figures 16c and d show the results of the fluorescence phase shift measurements for 280-nm and 365-nm excitation, respectively. In both cases, diesel fuels exhibit much larger phase shifts in comparison with those of the spores.

Fluorescence spectra of *B. globigii* spores are compared with those of the building materials in Fig. 17a to c. Under 280-nm excitation (solid lines), chalk (Fig. 17b) exhibits a broad band in the blue to green region peaked at about 490 nm and a less intense band in the near-UV region at about 350 nm. Gypsum plaster (Fig. 17c) shows an asymmetric band peaked at bout 450 nm and a somewhat lower UV shoulder. A characteristic feature of these spectra is a relatively low ratio of near-UV to blue-green emission intensities in comparison to that of *B. globigii* spores. When the excitation wavelength is shifted to 365 nm, fluorescence spectra of the building materials in the blue-green region (dashed lines in Fig. 17 b and c) undergo almost no changes in comparison with those under deep-UV excitation and are very similar to the blue-green fluorescence spectrum of *B. globigii* spores.

Comparison of the fluorescence phase shift in the spores with that in the building materials under 280-nm excitation (Fig. 17d) shows a strong overlap with chalk and a somewhat smaller phase shift in gypsum plaster. For 365-nm excitation (Fig. 17e), the phase shifts of the both building materials remain almost unchanged, whereas a pronounced drop in phase shift of *B. globigii* spores is observed. This drop can be used for the discrimination of *B. globigii* spores against the investigated building materials despite very similar fluorescence spectra.

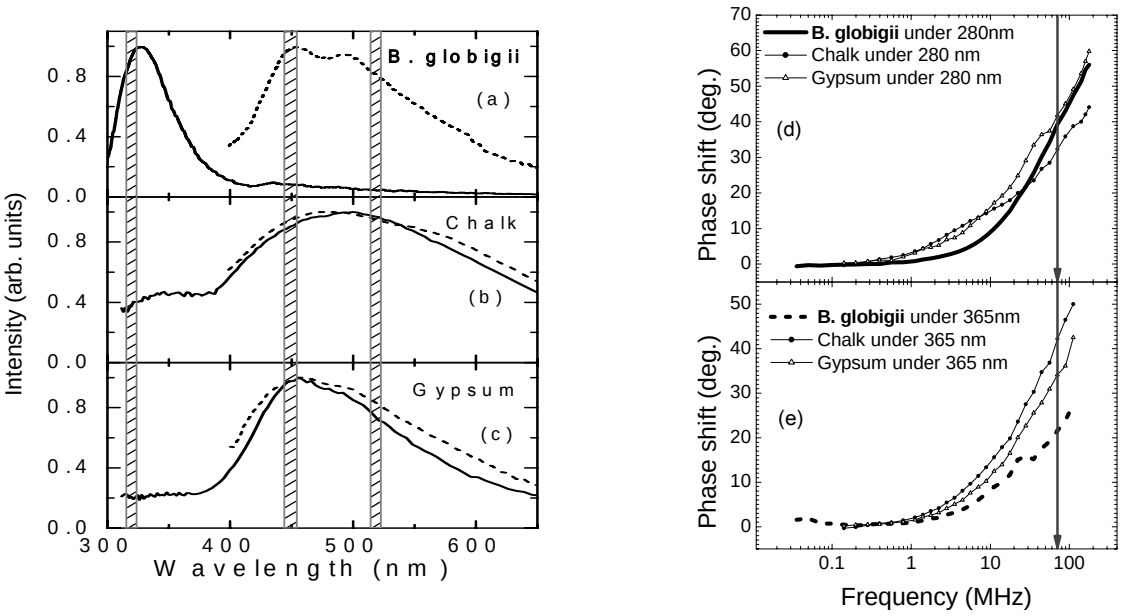

Fig. 17. Fluorescence spectra of *B. globigii* (a) vs. building materials chalk (b) and gypsum plaster (c) under 280-nm (solid lines) and 365-nm (dashed lines) excitations. Phase shift under 280-nm (c) and 365-nm (d) excitation as a function of frequency for *B. globigii* (solid line for 280-nm excitation, dashed line for 365-nm excitation), chalk (filled circles) and gypsum plaster (open triangles).

5.5. Discrimination charts and sensor concept

To design an optimal sensor, a set of the output parameters should be carefully selected to allow for high discrimination ability and reproducibility. Our selection of the set of output parameters was based on the following conditions. First, parameters, which combine data acquired using different excitation sources must be avoided because of different thermal drift and aging rate of the sources. Second, spectral signatures based on absolute fluorescence signals are inappropriate, since the detected intensity of the fluorescence signal depends on the size and number of the interrogated particles, contamination and aging of the optical components, and drift of output of the excitation sources. Contrarily, fluorescence-phase signatures, which are almost independent on the excitation power and sensitivity of the detector, can be employed as absolute quantities. Consequently, the sets

of the output parameters were built individually for each excitation source; they contain ratios of the fluorescence intensities and absolute values of the phase shits.

Of eight excitation wavelengths used for the generation of the data matrix of the fluorescence spectral and phase signatures, two excitation wavelengths, 280 nm and 365 nm, were selected as yielding the most discriminative data (see Section 5.4). Basing on the spectral peaks averaged over all materials investigated, fluorescence intensity in three spectral regions, around 320 nm, 450 nm, and 520 nm (shown by dashed areas in Figs. 13 to 17), were selected for use in the sensor output parameters. For the 280-nm LED, the corresponding output parameter was chosen as the ratio of fluorescence intensities at 320 nm and 450 nm, whereas for the 365-nm LED, the 450 nm to 520 nm intensity ratio was employed. Since these ratios vary within many orders of magnitude within the entire data matrix, a logarithmic presentation was used.

For the fluorescence decay signature, a single value of the fluorescence waveform phase shift in respect of the excitation one at a particular frequency and within a particular spectral window is sufficient to use as output parameter. Ideally, the most appropriate frequency for the highest discrimination of *B. globigii* against other fluorescent objects is that where the derivative of the phase shift vs. frequency dependence has the highest value, i.e. about 100 MHz where the phase shift is about 45 degrees (see Fig. 12a). However, because of many practical reasons (drop in the modulation ability of the LEDs, reduction of fluorescence modulation depth, and increase in parasitic electric crosstalk between the excitation and detection arms with frequency), a somewhat lower frequency is preferable. As a compromise, the frequency around 70 MHz was selected (vertical arrows in Figs. 13 to 17). For the 365-nm LED, the phase shift in the spectral window at 450 nm was employed, whereas for the 280-nm LED, of two possible spectral windows, only that at 320 nm was used. (As mentioned above, some materials under 280-nm excitation exhibit low fluorescence intensity in the 450-nm spectral window making measurements of the phase shift less accurate.)

Eventually, two-dimensional fluorescence discrimination charts were built for each of two excitation LEDs. Figure 18a shows the chart for the 280-nm LED with logarithm of the ratio of the fluorescence intensities at 320 nm and 450 nm standing for one coordinate and the phase shift at 71.8 MHz within the 320-nm spectral window standing for the second coordinate. Correspondingly, Fig. 18b shows the chart for the 365-nm LED. Here the horizontal coordinate is logarithm of the ratio of the fluorescence intensities at 450 nm and 520 nm, whereas the vertical coordinate is the phase shift at the same frequency within the 450-nm spectral window. Both charts are presented in the same scaling in order one could visually compare the discrimination ability for each excitation LED used. Fig. 18 clearly indicates that the ability of spectral discrimination of *B. globigii* spores against common interferants is much higher for excitation using the 280-nm LED than for the 365-nm one (*cf.* the span of the data along the horizontal axis in Figs. 18a and 18b). Also, the deep-UV LED shows somewhat higher span of the data along the vertical axis, i.e. discrimination in the fluorescence phase shift.

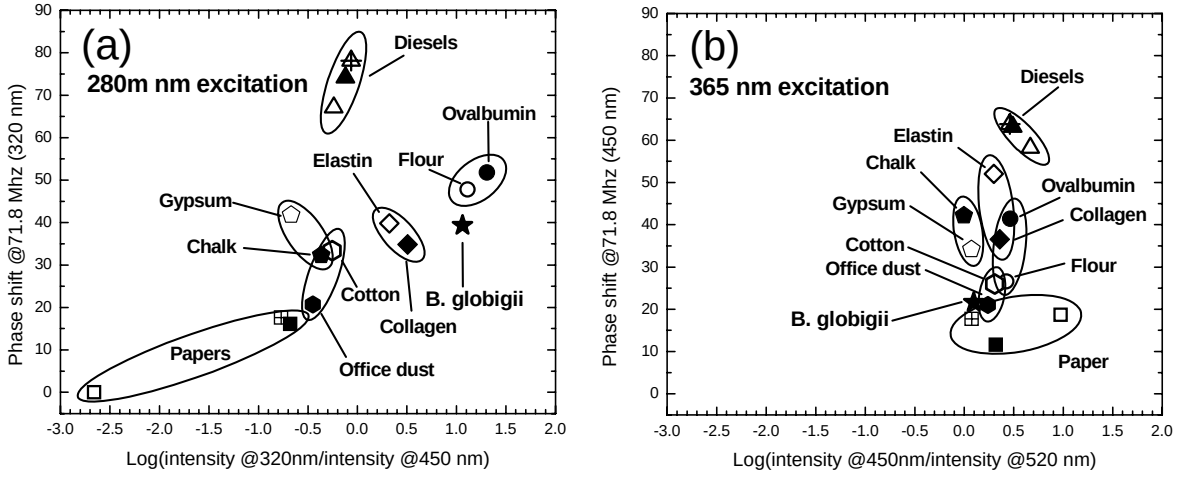

Fig. 18. (a) Distribution the fluorescence phase shift at 71.8 MHz vs. fluorescence intensity ratio at 320 nm and 450 nm for 280 nm excitation (a) and vs. fluorescence intensity ratio at 450 nm and 520 nm for 365-nm excitation (b).

To assess the applicability of the fluorescence spectral and phase signatures for use in a bioparticle sensor, we performed rating of the distances between the points corresponding to *B. globigii* and those nearest corresponding to various groups of interferants in Figs. 18a and 18b. Based on the reproducibility of the measurement data for *B. globigii* samples, differences in phase shift between 5 and 10 degrees were rated as

rendering “moderate” discrimination, whereas those above 10 degrees were rated for “high” discrimination. Accordingly, differences in the fluorescence intensity ratio between 2 and 5 times were rated as rendering “moderate” discrimination, whereas those exceeding 5 times were rated for “high” discrimination. Table 1 presents the summary of the ratings for the two excitation wavelengths (280 nm and 365 nm).

Table 1. Ratings of fluorescence spectral and phase signatures in discrimination of *B. globigii* spores against various groups of interferants for excitation using 280-nm and 365-nm LEDs.

	UV to blue intensity, 280 nm LED	UV phase, 280 nm LED	Blue to green intensity, 365 nm LED	Blue phase, 365 nm LED
B. globigii vs. cellulosous materials	high	moderate	low	low
B. globigii vs. epithelium materials	moderate	low	low	high
B. globigii vs. albumious materials	low	moderate	low	moderate
B. globigii vs. diesel fuels	high	high	moderate	high
B. globigii vs. building materials	high	low	low	high

Discrimination charts (Figs. 18a and b) and summary presented in Table 1 were used for designing of an optimal scheme of a “detect-to-warn” bioparticle sensor. The main optimization objectives we posed were as follows i) use as few excitation sources as possible; ii) use as few optical detection channels as possible; iii) achieve high discrimination ability against common interferants; iv) operate in real time.

Excitation sources. Table 1 shows that when both the spectral and phase-shift signatures are employed for discrimination of *B. globigii* against common interferants, 280-nm excitation exhibits at least one high or moderate rating for albuminous, epithelium, cellulosous, and building interferants and both high ratings for aromatic hydrocarbons. For 365-nm excitation, discrimination against epithelium materials is somewhat higher (low and high ratings vs. moderate and low), whereas both ratings for cellulosous materials ale low. This suggests that when the fluorescence spectral signature is complemented by the decay-time signature (phase shift), a single 280-nm excitation source is stringent and almost sufficient for excitation. Alternatively, Table 1 implies that at least one high or moderate discrimination rating for each group of interferants can be obtained in a measurement scheme based solely on fluorescence intensity ratios when two excitation sources (280 and 365 nm) and three detection channels (320 nm, 450 nm, and 520 nm) are used. However, a single-source approach has many advantages in respect of the conventional two-source (280/340 nm) scheme. First, the number of expensive optical elements for filtering and routing excitation and fluorescence can be reduced and substituted by potentially cheap electronic circuits for the LED modulation and fluorescence phase measurement. Second, use of a single source requires no sharing of measurement time and switching between the detection arms activated by different sources what simplifies the electronics and reduces the reaction time of the sensor. Third, issues due to different thermal and ageing drift of different sources (e.g., normalization procedures) are avoided.

Detection channels. For 280-nm excitation, the 320-nm spectral window is the most appropriate for fluorescence-phase discrimination of bacterial spores against most interferants. However, the phase-shift signature is insufficient for high discrimination against some interferants and must be supplemented by a spectral signature. The latter requires at least two detection channels. Of those, one can employ the same 320-nm window, whereas the most appropriate second spectral window lies in the blue region (around 450 nm). Therefore in a sensor with fluorescence-phase measurement employed, two optical detection channels are sufficient. Meanwhile in a high-performance fluorescent sensor based solely on fluorescence intensity ratios, at least three optical detection channels are required.[41]

Discrimination ability. Obviously for the same number of the excitation sources and optical detection channels, a sensor with fluorescence phase measurement should be superior in discrimination ability to a conventional one based solely on the measurement of fluorescence intensity owing to a larger number of the output parameters. Even more, the above considerations imply that a fluorescence-phase sensor with a reduced number of the excitation sources and optical detection channels has somewhat higher overall discrimination ability in comparison to a conventional sensor (4 high, 3 moderate, and 3 low ratings vs. 3 high, 2 moderate, and 5 low ratings). Actually, replacement of the green to blue fluorescence spectral signatures provided by the near-UV excitation source (340–365 nm) by a fluorescence-decay signature provided by the deep-UV excitation source (255–280 nm) results in an improvement in discrimination, especially between the particles that contain proteins and those that do not. The reason is in that protein emission in the 320-nm range is dominated by a single amino acid, tryptophan, with the fluorescence lifetime specific to local environment. Meanwhile spectral signatures in the blue-green spectral region are sensitive to the purity of bacterial agents and are difficult to

distinguish, especially when a bacterial agent is masked by interferants in particle mixtures that are usually interrogated in inexpensive LED-based sensors.

Real time operation. Basically, fluorescence lifetime signature can be obtained in either time domain (pulsed excitation) or frequency domain (harmonically modulated excitation). Both of two modes have advantages and disadvantages in respect of each other[10] (see also Section 2.2). For research applications, the advantage of time-domain measurement is the direct acquisition of the temporal decay profile, which is very convenient, rather than of a phase vs. frequency dependence, which is a Fourier transform of the time dependence. Fortunately, for sensor applications this is not important, since both the decay time and phase shift are interconvertible unique signatures of a fluorophore. However for a sensor operating in real time, the frequency domain mode is more appropriate, since the measurement can be continuous without a need of separate stages of data accumulation and processing as in the time-domain mode. Also in the frequency-domain measurement mode, the fluorescence intensity and phase can be independently measured at the same time within one detection channel by simple branching of the dc and ac components of the photocurrent. Finally in the time domain mode, pulsed excitation requires high peak power that can result in artifacts due to the optical damage of the sample. These considerations infer that for real-time operation, use of the frequency-domain mode is preferable. However, further development of the frequency-domain technique is needed to catch up with the pulsed methods in terms of sensitivity. In particular, a method of phase shift measurement in the photon counting mode analogous to the time-correlated photon counting, which is widely used in the time-domain fluorescence lifetime measurements, is to be developed.

A simple scheme of a concept bioparticle sensor, which utilizes the fluorescence decay time signature, is presented in Fig. 19. The sensor contains a single excitation source, 280-nm LED that is modulated at a frequency of about 70 MHz using a harmonic oscillator. The emission of the LED is filtered by a SPF to improve the spectral purity. A sample accumulation unit is to be used to preselect airborne particles within a particular range of sizes using elastic scattering of light and to collect them on a non-fluorescent substrate. Fluorescence is detected in two channels that are equipped with LPFs designed for the 320-nm and 450-nm spectral windows, respectively. In the 450-nm channel, the photodetector (PMT) is used just for the fluorescence intensity measurement, whereas in the 320-nm channel the photocurrent is split in to the dc and ac components that are used for the measurement of the fluorescence intensity and phase, respectively. Two logarithmic amplifiers and a subtractor are used to output the ratio of the intensities and a phase meter provides with a signal related to the phase difference between the waveforms of the driving oscillator and fluorescence in the 320-nm channel. The sensor operates in a continuous regime and alarms when the two output signals synchronously fall within the ranges specific for a hazardous biological agent.

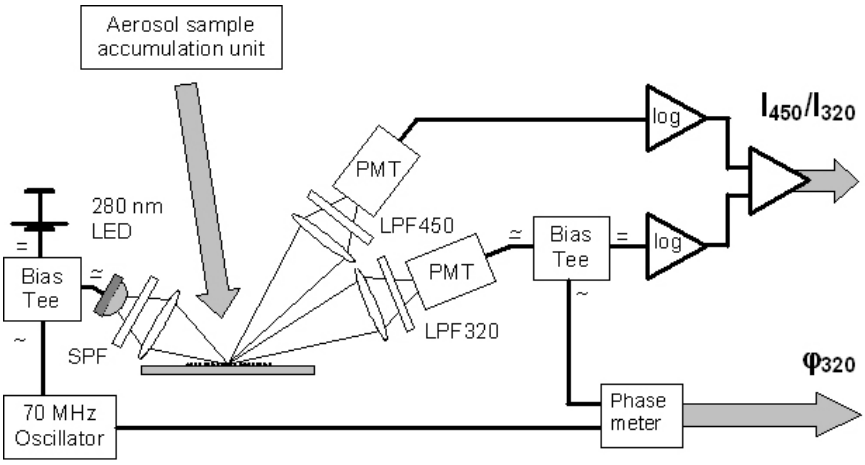

Fig. 19. Schematic presentation a proposed single-source biofluorescence sensor utilizing fluorescence spectral and phase signatures.

6. CONCLUSIONS

1. Spectral purity of the emission and high-frequency modulation ability of UV AlGaN LEDs (255–340 nm, SETI) developed under SUVOS program as well as of commercial InGaN LEDs (365–375 nm, Nichia) were tested for the applicability in fluorescence lifetime measurement in the frequency domain. For AlGaN-based

LEDs, the high-contrast emission spectra exhibited peak-to-background ratio of about 4 orders of magnitude, which is sufficient for sensitive fluorescence measurements using colored-glass and interference optical filters. The cut-off frequency of the AlGaN LEDs investigated was in the range above 100 MHz, which allow for measurements of fluorescence decay lifetime with a subnanosecond resolution using a frequency-domain method. The InGaN LEDs exhibited almost same spectral purity and lower cut-off frequencies (~ 20 MHz).

2. A laboratory facility for frequency-domain measurements of fluorescence lifetime using UV LEDs was optimized. Sets of mutually extinguishing pairs of optical filters and dichroic filters for optical isolation of the excitation and detections arms of the facility were developed and the sensitivity of the detection was improved by using an additional wide-band amplifier. A LabVIEW tool was created to automate the measurement procedure and to process the data. The facility was verified by measurements of fluorescence phase shift and modulation depth in the frequency-domain (0.1 to 200 MHz) in standard fluorophores (organic dyes and their mixtures). Single-exponent and multi-exponent fluorescence decay patterns were revealed in the nanosecond range to assess the sensitivity and accuracy of the measurement technique. Fluorescence lifetime was shown to be resolved with an accuracy of about 3% for fluorophore concentrations as low as 5×10^{-8} mol/l what is sufficient to distinguish between different chemical and biological compounds.
3. A set of UV light-emitting diodes (LEDs) with the peak wavelengths ranging from 255 nm to 375 nm was applied for the investigation of spectral and decay-time fluorescence signatures in dry *B. globigii* spores, natural autofluorophores and common organic and inorganic airborne interferants (albuminous, epithelium, and cellulosous materials as well as aromatic hydrocarbons and mineral building materials). The fluorescence decay signature was represented by a phase shift of the sinusoidal fluorescence waveform in respect of excitation provided by high-frequency modulated LEDs.
4. The analysis of the matrix of fluorescence spectral and phase signatures of *B. globigii* spores and common interferants under excitation by LEDs with different emission wavelengths enabled us to propose a new concept of a "detect-to-warn" biofluorescence sensor. In its simplest implementation, the sensor contains a single excitation source, a 280-nm LED harmonically modulated at about 70 MHz frequency, and two photodetectors operating within the 320-nm and 450-nm spectral windows. The outputs of the sensor are the ratio of the fluorescence intensities in the two channels and the phase shift of the sinusoidal fluorescence waveform in respect of the excitation one in the 320-nm channel. In comparison with a conventional approach based just on the fluorescence intensity measurement, the proposed fluorescence-phase sensor features a lower number of expensive optical elements and a potentially higher ability of discrimination of bioparticles against most common interferants (albuminous, epithelium, and cellulosous materials as well as aromatic hydrocarbons and mineral building materials).

REFERENCES

1. J. C. Carrano and A. J. Maltenfort, "Semiconductor ultraviolet sources for biological agent detection," *Proc. SPIE* **4743**, pp. 261–267, 2002.
2. *Optically Based Biological and Chemical Sensing for Defence*, ed. by J. C. Carrano and A. Žukauskas, *Proc. SPIE* **5617**, 2004.
3. R. G. Pinnick, S. C. Hill, S. Niles, D. M. Garvey, Y.-L. Pan, S. Holler, R. K. Chang, J. Bottiger, B. V. Bronk, B. T. Chen, C.-S. Orr, and G. Feather, "Real-time measurement of fluorescence spectra from single airborne biological particles," *Field Anal. Chem. Technol.* **3**, pp. 221–239, 1999.
4. V. Sivaprakasam, A. L. Huston, C. Scotto, and J. D. Eversole, "Multiple UV wavelength excitation and fluorescence of bioaerosols," *Optics express* **12**, pp. 4457–4466, 2004.
5. *UV Solid-State Light Emitters and Detectors.* Proc. NATO ARW, Series II, Vol. 144, ed. by M. S. Shur and A. Žukauskas, Kluwer, Dordrecht, 2004.
6. M. Asif Khan, M. Shatalov, H. P. Maruska, H. M. Wang, and E. Kuokstis, "III-nitride UV devices," *Jpn. J. Appl. Phys.* **44**, pp. 7191–7206, 2005.
7. T. H. Jeys, L. Desmarais, E. J. Lynch, and J. R. Ochoa, "Development of a UV LED based biosensor," *Proc. SPIE* **5071**, pp. 234–240, 2003.
8. C. Call and E. Merrill, "AirSentinel®: A real-time bioaerosol monitor," *Proc. SPIE* **5617**, pp. 53–59, 2004.
9. J. Cabalo, R. Sickenberger, W. Underwood, and D. Sickenberger, "Micro-UV detector," *Proc. SPIE* **5617**, pp. 75–86, 2004.
10. J. R. Lakowicz, *Principles of Fluorescence Spectroscopy* (Kluwer/Plenum, New York, 1999).
11. P. Jonsson, F. Kullander, M. Nordstrand, T. Tjärnhage, P. Wästerby and M. Lindgren, "Development of fluorescence-based point detector for biological sensing," *Proc. SPIE* **5617**, pp. 60–74, 2004.
12. A. Žukauskas, M. S. Shur, and R. Gaska, *Introduction to Solid-State Lighting* (Wiley, New York, 2002).

13. T. Iwata, A. Hori and T. Kamada, “Photon-counting phase-modulation fluorometer,” *Opt. Rev.* **8**, pp. 326–329, 2001.
14. H. Peng, E. Makarona, Y. He, Y.-K. Song, A. V. Nurmikko, J. Su, Z. Ren, M. Gherasimova, S.-R. Jeon, G. Cui, and J. Han, “Ultraviolet light-emitting diodes operating in the 340 nm wavelength range and application to time-resolved fluorescence spectroscopy,” *Appl. Phys. Lett.* **85**, pp. 1436–1438, 2004.
15. C. D. McGuinness, K. Sagoo, D. McLoskey and D. J. S. Birch, “A new sub-nanosecond LED at 280 nm: application to protein fluorescence,” *Meas. Sci. Technol.* **15**, pp. L19–L22, 2004.
16. C. D. McGuinness, K. Sagoo and D. McLoskey, D. J. S. Birch, “Selective excitation of tryptophan fluorescence decay in proteins using a subnanosecond 295 nm light-emitting diode and time-correlated single-photon counting,” *Appl. Phys. Lett.* **86**, article No 261911, 2005.
17. P. Vitta, N. Kurilcik, A. Novickovas, S. Jursenas, H. Calkauskas, A. Zukauskas, and R. Gaska, “AlGaN-based deep UV LEDs for fluorescence sensing,” *Proc. SPIE* **5617**, pp. 347–353, 2004.
18. P. Vitta, N. Kurilčik, S. Juršėnas, A. Žukauskas, A. Lunev, Y. Bilenko, J. Zhang, X. Hu, J. Deng, T. Katona, and R. Gaska, “Deep-UV light-emitting diodes for frequency-domain measurements of fluorescence lifetime in basic biofluorophores,” *Appl. Phys. Lett.* **87**, article No 084106, 2005.
19. P. Vitta, N. Kurilčik, S. Juršėnas, A. Žukauskas, E. Bakienė, J. Zhang, T. Katona, Y. Bilenko, A. Lunev, X. Hu, J. Deng, and R. Gaska, “Fluorescence-lifetime identification of biological agents using deep ultraviolet light-emitting diodes,” *Proc. SPIE* **5990**, pp. X-1–X-14, 2005.
20. J. P. Zhang, A. Chitnis, V. Adivarahan, S. Wu, V. Mandavilli, R. Pachipulusu, M. Shatalov, G. Simin, J. W. Yang, and M. Asif Khan, “Milliwatt power deep ultraviolet light-emitting diodes over sapphire with emission at 278 nm,” *Appl. Phys. Lett.* **81**, pp. 4910–4912, 2002.
21. V. Adivarahan, S. Wu, J. P. Zhang, A. Chitnis, M. Shatalov, V. Mandavilli, R. Gaska, M. A. Khan, “High-efficiency 269 nm emission deep ultraviolet light-emitting diodes,” *Appl. Phys. Lett.* **84**, pp. 4762–4764, 2004.
22. W. H. Sun, J. P. Zhang, V. Adivarahan, A. Chitnis, M. Shatalov, S. Wu, V. Mandavilli, J. W. Yang, and M. A. Khan, “AlGaN-based 280 nm light-emitting diodes with continuous wave powers in excess of 1.5 mW,” *Appl. Phys. Lett.* **85**, pp. 531–533, 2004.
23. J. P. Zhang, X. Hu, Yu. Bilenko, J. Deng, A. Lunev, M. S. Shur, R. Gaska, M. Shatalov, J. W. Yang, and M. A. Khan, “AlGaN-based 280 nm light-emitting diodes with continuous-wave power exceeding 1 mW at 25 mA,” *Appl. Phys. Lett.* **85**, pp. 5532–5534, 2004.
24. S. L. Rumyantsev, S. Sawyer, M. S. Shur, N. Pala, Yu. Bilenko, J. P. Zhang, X. Hu, A. Lunev, J. Deng, and R. Gaska, “Low-frequency noise of GaN-based ultraviolet light-emitting diodes,” *J. Appl. Phys.* **97**, article No 123107, 2005.
25. P. Harms, J. Sipior, N. Ram, G. M. Carter, and G. Rao, “Low cost phase-modulation measurements of nanosecond fluorescence lifetimes using a lock-in amplifier,” *Rev. Sci. Instrum.* **70**, pp. 1535–1539, 1999.
26. L. Rosso and V. C. Fernicola, “Time- and frequency-domain analyses of fluorescence lifetime for temperature sensing,”*Rev. Sci. Instrum* **77**, article No 034901, 2006.
27. S. Sarasanandarajah, J. Kunnil, B. V. Bronk, and L. Reinisch, “Two-dimensional multiwavelength fluorescence spectra of dipicolinic acid and calcium dipicolinate,” *Appl. Opt.* **44**, pp. 1182**–** 1187, 2005.
28. L. Callegaro and E. Puppin, “Lasers and light-emitting diodes as sources for fixed-wavelength magneto-optical phase modulated ellipsometry,” *Rev. Sci. Instrum.* **66**, pp. 5375–5376, 1995.
29. A. Žukauskas, A. Novičkovas, P. Vitta, M. S. Shur, and R. Gaska, “Raman measurements in water using a high-power light-emitting diode,” *J. Raman Spetrosc.* **34**, pp. 471–473, 2003.
30. S. Machida, Y. Yamamaoto, and Y. Itaya, “Observation of amplitude squeezing in a constant-current-driven semiconductor laser,” *Phys. Rev. Lett.* **58**, pp. 1000–1003, 1987
31. W. L. Nicholson and P. Setlow, “Sporulation, germination and out-growth,” in *Molecular biological methods for Bacillus*, ed. by C. R. Harwood and S. M. Cutting, Wiley, Chichester, 1990, pp. 391–450.
32. T. J. Leighton and R. H. Doi, “The stability of messenger ribonucleic acid during sporulation in *Bacillus subtilis*,” *J. Biol. Chem*. **246**, pp. 3189–3195, 1971.
33. A. S. Ladokhin, “Fluorescence spectroscopy in peptide and protein analysis,” in *Encyclopedia of Analytical Chemistry*, ed. by R. A. Meyers, Wiley, Chichester, 2000, pp. 5762–5779.
34. R. Nudelman, B. V. Bronk, and S. Efrima “Fluorescence emission derived from dipicolinic acid, its sodium, and its calcium salts,” *Appl. Spectrosc.* **54**, pp. 445–449, 2000.
35. *Handbook of Biomedical Fluorescence*, ed. By M.-A. Mycek, B. W. Pogue, Marcel Dekkek, Inc., New York, 2003.
36. A. P. Demchenko, *Ultraviolet Spectroscopy of Proteins*, Springer Verlag, New York, 1981.
37. K. Guzow, R. Ganzynkowicz, A. Rzeska, J. Mrozek, M. Szabelski, J. Karolczak, A. Liwo, and W. Wiczk, “Photophysical properties of tyrosine and its simple derivatives studied by time-resolved fluorescence spectroscopy, global analysis, and theoretical calculations,” *J. Phys. Chem. B* **108**, pp. 3879–3889, 2004.
38. J. A. Olmstead and D. G. Gray, “Fluorescence spectroscopy of cellulose, lignin, and mechanical pulps: A review,” *J. Pulp Paper Sci*. **23**, pp. J571–J581, 1997.
39. Z. Deyl, K. Macek, M. Adam, and O. Vancikova, “Studies on the chemical nature of elastin fluorescence,” *Biochim. Biophys. Acta.* **625**, pp. 248–541, 1980.
40. I. B. Berlman, *Handbook of fluorescence spectra of aromatic molecules*, Academic Press, London, 1971.
41. T. Pletcher, J. McGinn, D. Keller, A. Huston, J. Eversole, and V. Sivaprakasum, “Experimental performance of a novel aerosol sorting and deposition system for bio-treat sensing applications,” *Proc. SPIE* **6398**, pp. A1–A13, 2006.

PUBLICATIONS

Technical papers

1. A. Zukauskas, N. Kurilcik, P. Vitta, S. Jursenas, E. Bakiene, R. Gaska, “Optimization of a UV light-emitting diode based fluorescence phase sensor,” *Proc. SPIE* **6398**, pp. Y1–Y14, 2006.
2. A. Žukauskas, P. Vitta, N. Kurilčik, S. Juršėnas, and E. Bakienė, “Biological applications of frequency-domain fluorescence lifetime measurements using ultraviolet light-emitting diodes,” *Opt. Mater.*, 2007, in press.
3. A. Žukauskas, Phase-sensitive measurements of biofluorescence using deep ultraviolet light-emitting diodes, *Int. J. High Speed Electron. Syst.*, 2007, in press.

Conference presentations

1. P. Vitta, N. Kurilcik, S. Jursenas, A. Zukauskas, E. Bakiene, J. P. Zhang, T. Katona, Y. Bilenko, A. Lunev, X. Hu, J. Deng, and R. Gaska, “Deep ultraviolet light-emitting diodes for fluorescence decay measurements in bacterial fluorophores and biological agents,” *Int. Conf. Blue Lasers and Light Emitting Diodes ISBLLED2006. Programme and Abstract Book* (Montpellier, France, May 15–19, 2006), pp. 137–138.
2. A. Žukauskas, P. Vitta, N. Kurilčik, S. Juršėnas, and E. Bakienė, “Biological applications of frequency-domain fluorescence lifetime measurements using ultraviolet light-emitting diodes,” *Int. Workshop on Adv. Spectroscopy and Opt. Materials.Book of Abstracts* (Gdansk, Poland, June 11–14, 2006), p. 23.
3. A. Zukauskas, N. Kurilcik, P. Vitta, S. Jursenas, E. Bakiene, R. Gaska, “Optimization of a UV light-emitting diode based fluorescence phase sensor,” *Optically Based Biological and Chemical Sensing for Defence III. Abstract Summaries* (Stockholm, Sweden, September 11–14, 2006), p. 128. (invited).